ghrl$^{-/-}$ mice appeared grossly normal, undergoing normal development to reach adulthood. Male *ghrl*$^{+/+}$, *ghrl*$^{+/-}$, and *ghrl*$^{-/-}$ mice had similar body weights at all ages (Fig. 1A).

3.2. Feeding pattern of *ghrl*$^{-/-}$ mice

We hypothesized that ghrelin plays a major role in promoting appetite and regulating feeding patterns. To test this hypothesis, we tested if genetic deletion of ghrelin decreased food intake. When *ghrl*$^{-/-}$ mice were fed standard chow, we did not observe any significant differences in the cumulative food intake over 10 weeks between male *ghrl*$^{-/-}$ and *ghrl*$^{+/+}$ littermates (Fig. 1B). In addition, there were no significant differences in feeding patterns between *ghrl*$^{+/+}$ and *ghrl*$^{-/-}$ littermates, despite measurement of food intake every 15 min over 11 days using the K2-CABIN apparatus (Fig. 2A). *Ghrl*$^{-/-}$ mice ate higher quantities of food in dark phase than in light phase, which was similar to *ghrl*$^{+/+}$ littermates (Fig. 2B). These results indicate that ghrelin does not have an essential role in feeding patterns.

3.3. Adaptation capability to negative energy states of *ghrl*$^{-/-}$ mice

If ghrelin is necessary for the feeding behaviors induced by negative energy state, *ghrl*$^{-/-}$ mice may exhibit abnormal behaviors during scheduled feeding. Within one week, *ghrl*$^{+/+}$ and *ghrl*$^{-/-}$ littermates both adapted to scheduled feedings, consuming the same amount of food per day (Fig. 3). There were also no differences in water intake or body weight between the

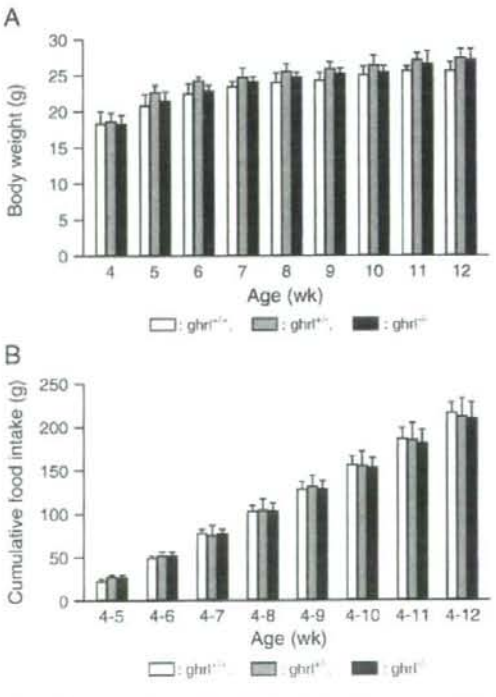

Fig. 1. *Ghrl*$^{-/-}$ mice exhibit normal growth rates and food intake. (A) Body weight; (B) cumulative food intake. Mice were four weeks old at the beginning of the study ($n=8$, $P>0.05$ [*ghrl*$^{+/+}$, *ghrl*$^{-/-}$ versus *ghrl*$^{+/-}$ mice]).

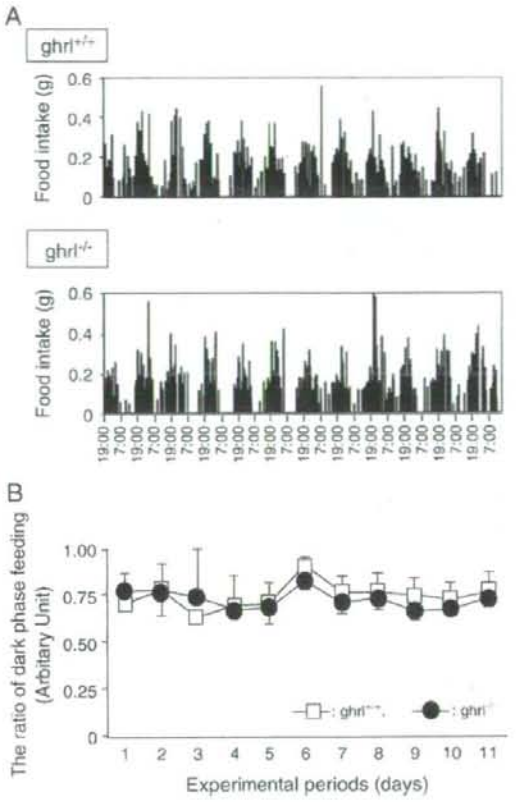

Fig. 2. *Ghrl*$^{-/-}$ mice display normal feeding patterns. (A) Food intake was recorded every 15 min for 11 days; (B) The ratio of dark phase feeding to total feeds ($n=6$, $P>0.05$ [*ghrl*$^{+/+}$ versus *ghrl*$^{-/-}$ mice]).

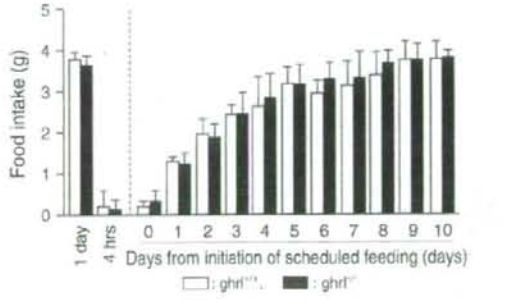

Fig. 3. The adaptation capability of *ghrl*$^{-/-}$ mice to a negative energy state is also normal ($n=6$, $P>0.05$ [*ghrl*$^{+/+}$ versus *ghrl*$^{-/-}$ mice]).

two groups (data not shown). These results demonstrate that *ghrl*$^{-/-}$ mice can adapt to a negative energy state.

3.4. Memory-related feeding performances of *ghrl*$^{-/-}$ mice

To test the physiologic role of ghrelin in feeding memory, we performed a food search test. Low values in *ghrl*$^{-/-}$ mice in comparison to *ghrl*$^{+/+}$ mice would indicate a critical role for ghrelin in this process. To test this assumption, we used a novel apparatus called KUROBOX. This apparatus has four food stations, named regions of interest (ROI), in the four corners of the cage (Fig. 4A). At any one time, however, the mouse can only take powder food from a single station. The correct food station rotated counter-clockwise every 4 h. To analyze the food searching behavior of mice, we used the correct visit ratio. This index is the ratio of visits to the correct ROI to the number of visits to all ROIs. In this experiment, the correct visit ratio was the same for *ghrl*$^{-/-}$ mice as that observed for *ghrl*$^{+/+}$ littermates; this index increased with time in both groups (Fig. 4B). Thus, *ghrl*$^{-/-}$ mice did not exhibit impaired feeding memory.

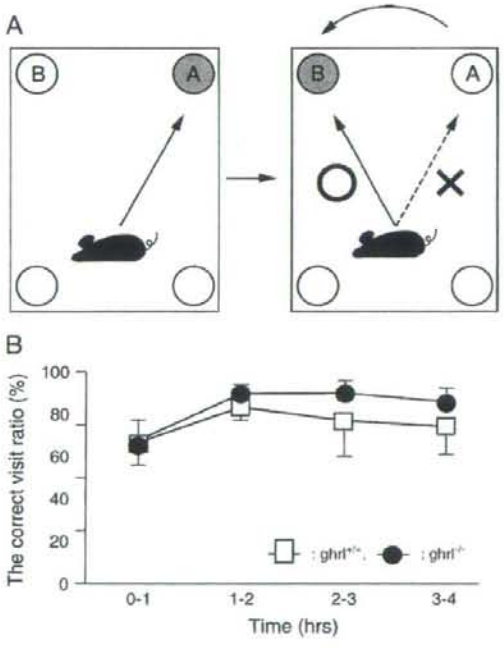

Fig. 4. The memory of feeding in *ghrl*$^{-/-}$ mice is normal. (A) Schematic illustration of the principles of KUROBOX analysis. When feed is first put in ROI A, the mouse always goes to ROI A to eat. Immediately after transferring feeds from ROI A to B, however, the mouse goes to ROI A by mistake at first. Gradually, the mouse goes to the correct ROI B. Investigation of the way of access can help estimate memory tasks in these mice. (B) The correct visit ratio is defined as the ratio of the number of visits to the correct food station to the number of visits to all stations ($n=6$, $P>0.05$ [*ghrl*$^{+/+}$ versus *ghrl*$^{-/-}$ mice]).

4. Discussion

Ghrelin has effects on puberty onset and pregnancy outcomes in rats [11]. Ghrelin also modulates rat testicular function and regulates gonadotropin secretion [12–14]. *Ghrl*$^{-/-}$ mice, however, were fertile and delivered normal litter sizes, indicating that ghrelin is not essential for reproductive function. While a number of reports indicate that ghrelin induces cell proliferation [15–17], there were no gross differences in tissue weights or body weights between *ghrl*$^{+/+}$ *and ghrl*$^{-/-}$ mice. There were no physical or tissue abnormalities identified in *ghrl*$^{-/-}$ mice by our routine analytical protocols. These results suggested that ghrelin is not critical for cell proliferation.

Centrally- or peripherally-injected ghrelin induces acute food intake in rats [18,19]. Ghrelin receptors localize in the SCN and the Arc, important regions in the regulation of circadian rhythms and feeding, respectively [4], suggesting that ghrelin maybe involved in feeding initiation and patterns. *Ghrl*$^{-/-}$ mice, however, have normal feeding patterns, with high food intake in dark phase and low intake in light phase. These results indicate that ghrelin is neither an initiator of feeding nor a regulator of feeding patterns. Ghrelin may act on the SCN to play an unknown role(s) in feeding patterns.

Fasting induces ghrelin secretion from the hypothalamus and stomach in rats [3]. Negative energy states induced by centrally-administered 2-deoxy-D-glucose also stimulates ghrelin secretion from the rat hypothalamus [3]. Plasma ghrelin levels are increased in anorexia nervosa patients and returns to basal levels following weight gain and recovery in these patients [20]. Patients with chronic heart failure (CHF) or chronic obstructive pulmonary disease (COPD) often exhibit a degree of cachexia. Plasma ghrelin levels were significantly higher in CHF patients with cachexia than those without cachexia [21]. Similarly, plasma ghrelin was elevated in underweight patients with COPD, in whom the levels were associated with a cachectic state [22]. Thus, ghrelin secretion is induced by negative energy states, suggesting that ghrelin is necessary for adaptation to negative energy states. In both *ghrl*$^{+/+}$ and *ghrl*$^{-/-}$ mice, however, the capacity to adapt to scheduled feeding was normal. Mice in both groups required approximately one week to eat the same amount of food during over one day. Thus, the absence of ghrelin does not physiologically change the scheduled feedings of mice.

Recently, ghrelin was shown to control hippocampal spine synapse density and memory performance [23]. Therefore, we investigated the memory-related feeding performance of *ghrl*$^{-/-}$ mice using the KUROBOX apparatus. This powerful tool allows us to analyze the memory of feeding. We could not, however, observe any differences in memory-related feeding performance between *ghrl*$^{+/+}$ and *ghrl*$^{-/-}$ mice. In both groups, the correct visit ratio increased with time after transfer of feedings. This result indicates that ghrelin does not control the food searching behaviors or the memory of feeding.

In summary, we did not observe any changes in the feeding performances of *ghrl*$^{-/-}$ mice in this study. Multiple previous reports have demonstrated that ghrelin has an important role in feeding regulation. Therefore, we cannot exclude the possibility that compensatory mechanisms may work to regulate feeding in

ghrl$^{-/-}$ mice. Although we also investigated the gene expression of a subset of orexigenic and anorexigenic peptides, we did not observe any differences between the two groups. It remains possible that an unknown mechanism regulates feeding. Thus, this study demonstrates that ghrelin is not critically required for feeding performance. Further studies will be needed to reveal the essential role(s) of ghrelin in these animals.

Acknowledgments

We thank Y. Yamashita and Y. Yoshida (Kurume University), and A. Kawai and Y. Maruyama (Osaka University) for their helpful assistance.

The studies in the authors' laboratory are supported by grants from Research on Measures for Intractable Diseases from the Health and Labour Sciences Research Grants, the MEXT Open Research Center Project (2004). And this work was supported in part by the Promotion of Basic Research Activities for Innovative Biosciences (PROBRAIN) (to M.K.), by Grant-in-Aids for Scientific Research from the Ministry of Education, Culture, Sports, Science and Technology of Japan (to M.K.), by Kato Memorial Bioscience Foundation (to T.S.), by The Foundation for Growth Science (to T.S.), and by the Sasakawa Scientific Research Grant (to T.S).

References

[1] Kojima M, Hosoda H, Date Y, Nakazato M, Matsuo H, Kangawa K. Ghrelin is a growth-hormone-releasing acylated peptide from stomach. Nature 1999;402:656–60.

[2] Dezaki K, Yada T. Ghrelin in the regulation of glucose and lipid metabolism. Nippon Rinsho 2004;62(Suppl 9):388–91.

[3] Sato T, Fukue Y, Teranishi H, Yoshida Y, Kojima M. Molecular forms of hypothalamic ghrelin and its regulation by fasting and 2-deoxy-D-glucose administration. Endocrinology 2005;146:2510–6.

[4] Zigman JM, Jones JE, Lee CE, Saper CB, Elmquist JK. Expression of ghrelin receptor mRNA in the rat and the mouse brain. J Comp Neurol 2006;494:528–48.

[5] Kamegai J, Tamura H, Shimizu T, Ishii S, Sugihara H, Wakabayashi I. Chronic central infusion of ghrelin increases hypothalamic neuropeptide Y and agouti-related protein mRNA levels and body weight in rats. Diabetes 2001;50:2438–43.

[6] Goto M, Arima H, Watanabe M, Hayashi M, Banno R, Sato I, et al. Ghrelin increases neuropeptide Y and agouti-related peptide gene expression in the arcuate nucleus in rat hypothalamic organotypic cultures. Endocrinology 2006;147:5102–9.

[7] Toshinai K, Date Y, Murakami N, Shimada M, Mondal MS, Shimbara T, et al. Ghrelin-induced food intake is mediated via the orexin pathway. Endocrinology 2003;144:1506–12.

[8] Cowley MA, Cone RD, Enriori P, Louiselle I, Williams SM, Evans AE. Electrophysiological actions of peripheral hormones on melanocortin neurons. Ann N Y Acad Sci 2003;994:175–86.

[9] Sato T, Yamaguchi T, Matsuzaki M, Satoh T, Suzuki A. Mammosomatotrophs develop within mammotroph clusters in bovine adenohypophysis. Tissue Cell 1999;31:499–504.

[10] Kurokawa M, Fujimura K, Sakurai-Yamashita Y. A new-generation apparatus for studying memory-related performance in mice. Cell Mol Neurobiol 2003;23:121–9.

[11] Fernandez-Fernandez R, Navarro VM, Barreiro ML, Vigo EM, Tovar S, Sirotkin AV, et al. Effects of chronic hyperghrelinemia on puberty onset and pregnancy outcome in the rat. Endocrinology 2005;146:3018–25.

[12] Furuta M, Funabashi T, Kimura F. Intracerebroventricular administration of ghrelin rapidly suppresses pulsatile luteinizing hormone secretion in ovariectomized rats. Biochem Biophys Res Commun 2001;288:780–5.

[13] Tena-Sempere M. Ghrelin: novel regulator of gonadal function. J Endocrinol Invest 2005;28:26–9.

[14] Tena-Sempere M, Barreiro ML, Gonzalez LC, Gaytan F, Zhang FP, Caminos JE, et al. Novel expression and functional role of ghrelin in rat testis. Endocrinology 2002;143:717–25.

[15] Kim SW, Her SJ, Park SJ, Kim D, Park KS, Lee HK, et al. Ghrelin stimulates proliferation and differentiation and inhibits apoptosis in osteoblastic MC3T3-E1 cells. Bone 2005;37:359–69.

[16] Nanzer AM, Khalaf S, Mozid AM, Fowkes RC, Patel MV, Burrin JM, et al. Ghrelin exerts a proliferative effect on a rat pituitary somatotroph cell line via the mitogen-activated protein kinase pathway. Eur J Endocrinol 2004;151:233–40.

[17] Duxbury MS, Waseem T, Ito H, Robinson MK, Zinner MJ, Ashley SW, et al. Ghrelin promotes pancreatic adenocarcinoma cellular proliferation and invasiveness. Biochem Biophys Res Commun 2003;309:464–8.

[18] Nakazato M, Murakami N, Date Y, Kojima M, Matsuo H, Kangawa K, et al. A role for ghrelin in the central regulation of feeding. Nature 2001;409:194–8.

[19] Date Y, Murakami N, Toshinai K, Matsukura S, Niijima A, Matsuo H, et al. The role of the gastric afferent vagal nerve in ghrelin-induced feeding and growth hormone secretion in rats. Gastroenterology 2002;123:1120–8.

[20] Cuntz U, Fruhauf E, Wawarta R, Tschop M, Folwaczny C, Riepl R, et al. A role for the novel weight-regulating hormone ghrelin in anorexia nervosa. Am Clin Lab 2002;21:22–3.

[21] Nagaya N, Uematsu M, Kojima M, Date Y, Nakazato M, Okumura H, et al. Elevated circulating level of ghrelin in cachexia associated with chronic heart failure: relationships between ghrelin and anabolic/catabolic factors. Circulation 2001;104:2034–8.

[22] Itoh T, Nagaya N, Yoshikawa M, Fukuoka A, Takenaka H, Shimizu Y, et al. Elevated plasma ghrelin level in underweight patients with chronic obstructive pulmonary disease. Am J Respir Crit Care Med 2004;170:879–8782.

[23] Diano S, Farr SA, Benoit SC, McNay EC, da Silva I, Horvath B, et al. Ghrelin controls hippocampal spine synapse density and memory performance. Nat Neurosci 2006;9:381–8.

Long-term trends of the incidence of hepatocellular carcinoma in the Nagasaki prefecture, Japan

NAOTA TAURA[1], HIROSHI YATSUHASHI[1], KAZUHIKO NAKAO[2], TATSUKI ICHIKAWA[2] and HIROMI ISHIBASHI[1]

[1]Clinical Research Center, National Nagasaki Medical Center, Kubara 2-1001-1, Omura, Nagasaki 856-8562; [2]The First Department of Internal Medicine, Nagasaki University School of Medicine, Sakamoto 1-7-1, Nagasaki 852-8501, Japan

Received April 14, 2008; Accepted August 4, 2008

DOI: 10.3892/or_00000212

Abstract. The incidence of hepatocellular carcinoma (HCC) in Japan is still increasing. The aim of the present study was to analyze the epidemiological trend of HCC in the Western area of Japan, Nagasaki. A total of 1,807 patients with HCC diagnosed at our two hospitals between 1981 and 2005 were consecutively recruited for this study. Cohorts of patients with HCC were categorized into five-year intervals. The etiology of HCC was categorized into four groups: HCC-B: HBsAg positive, HCVAb negative, HCC-C: HCVAb positive, HBsAg negative, HCC-BC: both of HBsAg and HCVAb positive and HCC-nonBC: both of HBsAg and HCVAb negative. The number and proportion of HCC-B cases decreased from 1986 to 1990 and thereafter stabilized, whereas those of HCC-C reached the peak from 1995 to 2000 and thereafter decreased. On the other hand, the number and ratio of the HCC-nonBC cases continued to increase in the whole period. The male/female ratio of HCC-C patients decreased from 6.4 in the period 1981-1985 to 1.9 in 2001-2005, indicating clearly the increase of female patients. On the other hand, the male/female ratio of other types of HCC patients did not change during the period. HCC patients rapidly increased from 1981 to 2000 and this increase was originated from that of HCC-C. The increase of the median age and the number of female patients with HCC-C was also demonstrated. The increase in the number and the proportion of the HCC-nonBC patients was also significant.

Introduction

Primary liver cancer is the most common primary cancer of the liver accounting for ~6% of all human cancers. It is estimated that half a million cases occur worldwide annually, making primary liver cancer the fifth most common malignancy in men and the ninth in women (1-6). Hepatocellular carcinoma (HCC) accounts for 85 to 90% of primary liver cancers (7) and the age-adjusted HCC mortality rate has increased in recent decades in Japan (8). Similarly, a trend of increasing rates of HCC has been reported from several developed countries in North America, Europe and Asia (9,10). HCC often develops in patients with liver cirrhosis caused by hepatitis B virus (HBV), hepatitis C virus (HCV), excessive alcohol consumption, or nonalcoholic fatty liver disease. Of the hepatitis viruses which cause HCC, HCV is predominant in Japan (11-14).

Although the age-adjusted incidence of HCC has increased in Japan, sequential changes in background features of HCC patients are not fully understood (15). Yoshizawa reports that deaths due to HCC in Japan have continued to increase in males, particularly in those older than 60 years of age in the past 3 decades, although the reasons for this are unclear (16). To clarify factors affecting epidemiological changes in Japanese HCC patients, especially the change in age distribution and gender, we analyzed the underlying features of HCC patients in a two major liver center-based study.

Patients and methods

Patients. A total of 1,807 patients with HCC diagnosed between January 1981 and December 2005 in the Liver Disease Center, National Nagasaki Medical Center and in the outpatient clinic of The First Department of Internal Medicine, Nagasaki University Hospital, were consecutively recruited for this study. The diagnosis of HCC was based on AFP levels and imaging techniques including ultrasonography (USG), computerized tomography (CT), magnetic resonance imaging (MRI), hepatic angiography (HAG) and/or tumor biopsy. The diagnostic criteria for HCC were either a confirmative tumor biopsy or elevated AFP (≥20 ng/ml) and neovascularization in HAG and/or CT. Cohorts of patients with HCC were categorized into five-year intervals (1981-1985, 1986-1990, 1991-1995, 1996-2000 and 2001-2005).

Etiology of HCC. Sera were stored at -80˚C until use. A diagnosis of chronic HCV infection was based on the presence of HCVAb (microparticle enzyme immunoassay; Abbott

Correspondence to: Dr Naota Taura, Clinical Research Center, National Nagasaki Medical Center, Kubara 2-1001-1, Omura, Nagasaki 856-8562, Japan
E-mail: ntaura@nmc-research.jp

Key words: hepatitis C virus, hepatocellular carcinoma, aging, Japan

Table I. The characteristics of HCC patients, 1981-2005.

Period	1981-1985	1986-1990	1991-1995	1996-2000	2001-2005	Total
Number	240	316	369	419	463	1807
Gender						
Male	194	257	268	314	314	1347
Female	46	59	101	105	149	460
Ratio (male/female)	4.2	4.4	2.7	3.0	2.1	2.9
Age (y.o) (IQR)	57 (6.5)	61 (5.1)	63 (5.4)	66 (5.1)	68 (6.3)	64 (6.5)
Hepatitis virus						
HCC-B	95	70	80	67	100	412
HCC-C	111	213	240	292	278	1134
HCC-B+C	8	8	9	11	10	46
HCC-nonBC	26	25	40	49	75	215

Gender: 2000-2005 vs. 1981-1985 p=0.0003; 2000-2005 vs. 1986-1990 p≤0.0001; 2000-2005 vs. 1991-1995 p=0.1330; 2000-2005 vs. 1996-2000 p=0.0197. Age: 2000-2005 vs. 1981-1985 p≤0.0001; 2000-2005 vs. 1986-1990 p≤0.0001; 2000-2005 vs. 1991-1995 p≤0.0001 and 2000-2005 vs. 1996-2000 p=0.0292. IQR, interquartile range.

Laboratories) and HCV-RNA detected by polymerase chain reaction (PCR), whereas diagnosis of chronic HBV infection was based on the presence of hepatitis B surface antigen (HBsAg) (enzyme-linked immunosorbent assay; Abbott Laboratories).

Statistical analysis. The data were analyzed by the Mann-Whitney test for the continuous ordinal data between two qualitative variables. The standard deviation was calculated based on the binomial model for the response proportion. $P<0.05$ was considered statistically significant.

Results

Clinical features of the studied patients. A total of 1,807 patients with HCC were diagnosed at our hospital from 1981 to 2005. There were 1,347 male (75%) and 460 female (25%) patients, with a median age of 64 years. The proportion of patients diagnosed as HCC-B (HBV-associated: HBsAg positive, HCVAb negative) was 23% (412 of 1,807), whereas 63% (1,134 of 1,807) had HCC-C (HCV-associated: HCVAb positive, HBsAg negative) and an additional 3% (46 of 1,807) had HCC associated with both viruses. The remaining 215 patients (12%) showed both of the virus markers negative.

As shown in Table I and Fig. 1, the number and proportion of HCC-B cases decreased from 1986 to 1990 and thereafter stabilized, whereas those of HCC-C reached the peak in the period 1996-2000 and thereafter decreased. The number and proportion of the HCC-nonBC (HBsAg and HCVAb negative) cases continued to increase in the whole period.

Background features for patients with HCC. Fig. 2 shows the median age at diagnosis of HCC-B, HCC-C and HCC-nonBC in five-year intervals (1981-1985, 1986-1990, 1991-1995, 1996-2000 and 2001-2005). The median age of patients at diagnosis of HCC-C showed a steadily significant increase from 58 to 69 years of age during the period. The median age of patients with HCC-B and HCC-nonBC did not significantly change during the period.

Fig. 3 shows the age distribution of patients with HCC-B and HCC-C with the five 5-year intervals. There was no difference in the age distribution of patients with HCC-B during these periods. In contrast, HCC-C obviously had a trend to increase in the number of patients aged >65 years.

Table I shows that the male/female ratio of HCC patients decreased from 4.2 in the period 1981-1985 to 2.1 in 2001-2005, indicating clearly the increase of female patients. In analysis of patients in HCC-C, the male/female ratio in the periods 1981-1985, 1986-1990, 1991-1995, 1996-2000 and 2001-2005 were 6.4, 4.8, 2.5, 2.7 and 1.9, respectively (1981-1985 vs. 2001-2005, p≤0.0001) (Table II). The ratio became clearly smaller, indicates an increase in female patients with HCC-C. On the other hand, the male/female ratio of other types of HCC patients did not significantly change during the period.

Discussion

This was a two major liver center-based study designed to examine the sequential change in the background of HCC patients during the past 25 years, 1981-2005. More than 80% of our patients had chronic HBV or HCV infections. During the observation period, the number and proportion of HCC-B cases decreased in the period 1986-1990 and thereafter reached a plateau, whereas HCC-C reached a peak in the period 1995-2000 and thereafter slightly decreased. On the other hand, the number and the proportion of HCC-nonBC gradually increased in the periods of 1981-1985, 1986-1990, 1991-1995, 1996-2000 and 2001-2005 being 26 (11%), 25 (8%), 40 (11%), 49 (12%) and 75 (16%), respectively. Previous studies from Japan reported that the proportion of HCC-C had been increased and reached a plateau in the

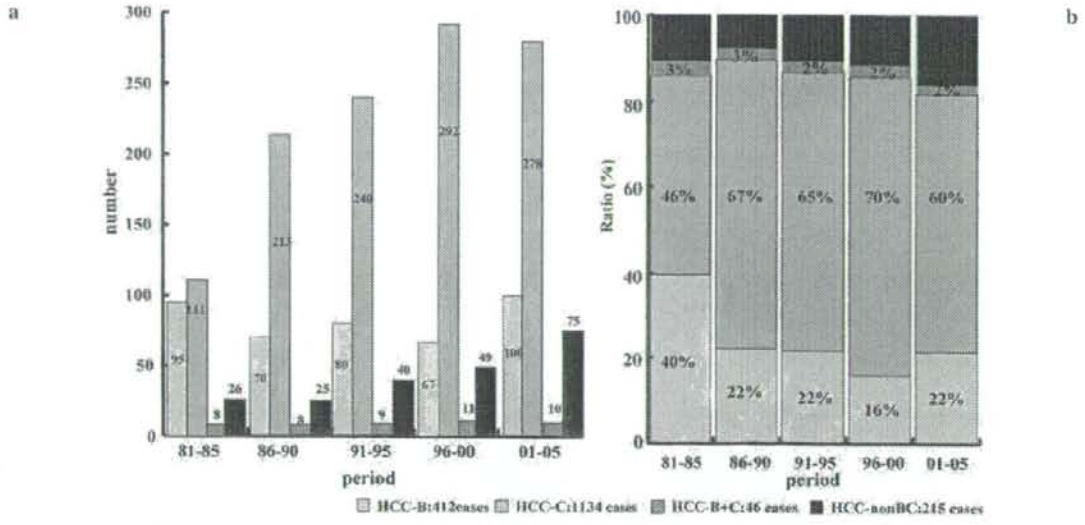

Figure 1. Sequential changes in the number (a) and ratio (b) of HCC patients categorized by etiology during the period 1981-2005 with 5-year intervals.

Table II. The number and male/female ratio of HCC patients during the period of 1981-2005.

Period	1981-1985	1986-1990	1991-1995	1996-2000	2001-2005	Total
Number	240	316	369	419	463	1807
Total						
Male	194	257	268	314	314	1347
Female	46	59	101	105	149	460
Ratio (male/female)	4.2	4.4	2.7	3.0	2.1	2.9
HCC-B						
Male	69	54	61	55	74	313
Female	26	16	19	12	26	99
Ratio (male/female)	2.7	3.4	3.2	4.6	2.9	3.2
HCC-C						
Male	96	176	172	212	182	838
Female	15	37	68	80	96	296
Ratio (male/female)	6.4	4.8	2.5	2.7	1.9	2.8
HCC-nonBC						
Male	21	20	29	40	51	1347
Female	5	5	11	9	24	460
Ratio (male/female)	4.2	4.0	2.6	4.4	2.1	2.9

HBV and nBnC: NS. HCV: 2000-2005 vs. 1981-1985 p≤0.0001; 2000-2005 vs. 1986-1990 p≤0.0001; 1996-2000 vs. 1981-1985 p=0.0033; 1996-2000 vs. 1986-1990 p=0.0084; 1991-1995 vs. 1981-1985 p=0.0024 and 1991-1995 vs. 1986-1990 p=0.0058.

period of 1981-2001 (8,15,17-19). However, in our study, the number and proportion of HCC-C cases decreased in the period 2001-2005. This may be due to interferon therapy associated with a decreased incidence of HCC (20-24). Iron depletion for chronic hepatitis C patients is a promising modality for lowering the risk of progression to HCC (25,26). Oral supplementation with oral branched-chain amino acids has been useful in the prevention HCC (27). Finally, the chronically HCV-infected population is aging in Japan. Yoshizawa reported that age-specific prevalence for the presence of HCVAb among ~300,000 voluntary blood donors from Hiroshima in 1999 clearly increased with the

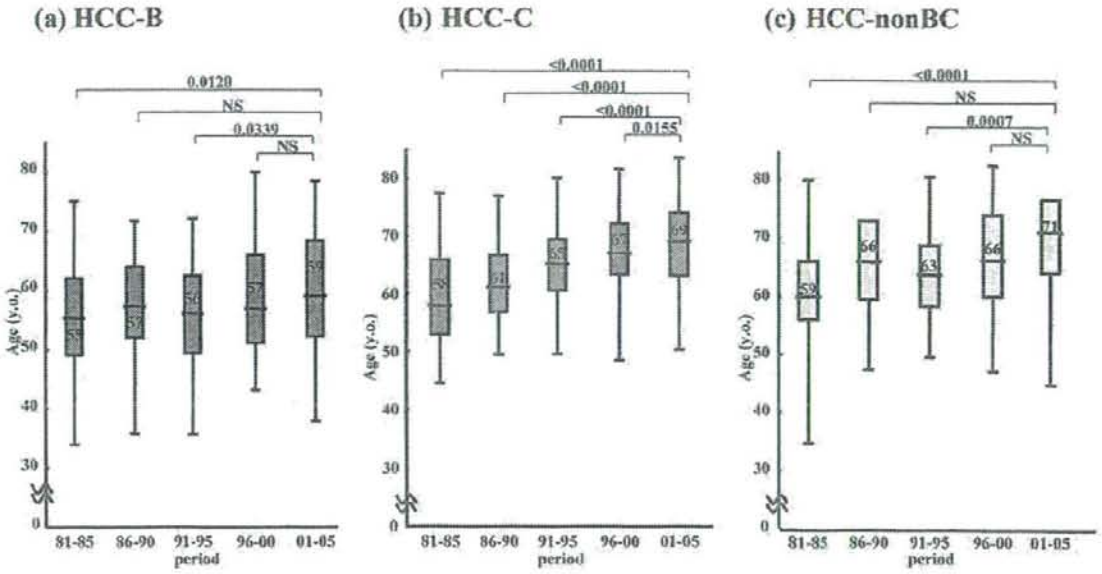

Figure 2. Sequential changes in the median age of HCC patients categorized by etiology during the period, 1981-2005 with 5-year intervals. (a) HCC-B, (b) HCC-C and (c) HCC-nonBC type p<0.05.

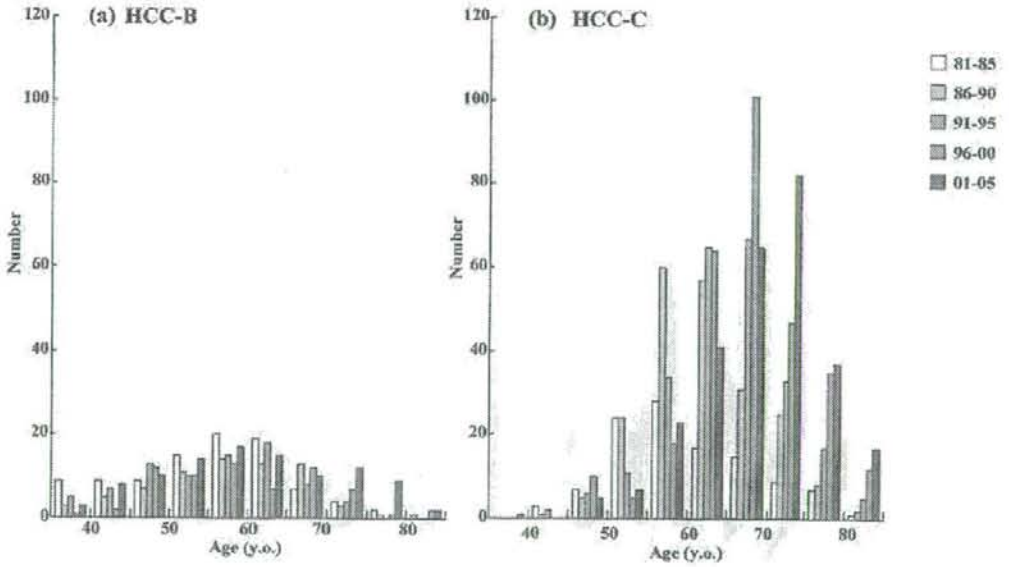

Figure 3. Changes in the age distribution of patients with HCC-B and HCC-C during the period, 1981-2005 with 5-year intervals.

age, reaching the highest proportion of 7% in individuals who were >70 years old (15,16). In this study, the median age of patients with HCC-C steadily increased from 58 to 69 years of age during the studied period, *i.e.* HCV infected people become older and they were regarded as a high risk for HCC.

In almost all populations, males have higher liver cancer proportions than females, with the male/female ratios usually averaging between 2:1 and 4:1 (7). However, the male/female ratio of HCC in Japan was 4.5 in the period 1983-1985 and 2.57 in 2000-2001 (17). In analysis of background features among HCC patients, HCC-B and HCC-nonBC cases revealed no significant change, whereas the male/female ratio of patients with HCC-C steadily decreased from 6.4 to 1.9 during the period. We suggest that the increase of female

patient with HCC-C was caused by the aging of HCV infected people. The increase of females among HCC patients was considered to increase because of HCC-C.

It is known that 2 to 4 decades of chronic HCV infection are required to develop cirrhosis and subsequent HCC (28-31). The number of HCC cases has increased in Japan, because individuals infected with HCV in the past have grown old and have reached the cancer-bearing age. The prevalence of HCV infection in young Japanese individuals is low and the incidence of HCVAb is very low because of preventative actions against HCV infection such as the screening of blood products for HCV and the use of sterile medical equipment (32). Additionally, we showed that the number and proportion of patients with HCC-C cases decreased together with an increase in the median age, whereas the number and ratio of HCC-nonBC steadily increased during the studied period. Based on these findings it may be expected that the incidence of HCC-nonBC in Japan may continue to increase even after the consequence of the HCV epidemic level off in the near future, although Japan is far advanced with regard to HCC-C.

In summary, HCC patients rapidly increased from 1981 to 2000 and this increase originated from HCC-C and the increase of the median age and the number of female patients with HCC-C. Increase in the number and proportion of the HCC-nonBC patients are also significant.

References

1. El-Serag HB and Mason AC: Risk factors for the rising rates of primary liver cancer in the United States. Arch Intern Med 160: 3227-3230, 2000.
2. El-Serag HB: Epidemiology of hepatocellular carcinoma. Clin Liver Dis 5: 87-107, 2001.
3. El-Serag HB, Hampel H, Yeh C and Rabeneck L: Extrahepatic manifestations of hepatitis C among United States male veterans. Hepatology 36: 1439-1445, 2002.
4. El-Serag HB: Hepatocellular carcinoma and hepatitis C in the United States. Hepatology 36: S74-S83, 2002.
5. El-Serag HB: Hepatocellular carcinoma: an epidemiologic view. J Clin Gastroenterol 35: S72-S78, 2002.
6. Hassan MM, Frome A, Patt YZ and El-Serag HB: Rising prevalence of hepatitis C virus infection among patients recently diagnosed with hepatocellular carcinoma in the United States. J Clin Gastroenterol 35: 266-269, 2002.
7. El-Serag HB and Rudolph KL: Hepatocellular carcinoma: epidemiology and molecular carcinogenesis. Gastroenterology 132: 2557-2576, 2007.
8. Kiyosawa K and Tanaka E: Characteristics of hepatocellular carcinoma in Japan. Oncology 62: 5-7, 2002.
9. McGlynn KA, Tsao L, Hsing AW, Devesa SS and Fraumeni JF Jr: International trends and patterns of primary liver cancer. Int J Cancer 94: 290-296, 2001.
10. Bosch FX, Ribes J, Diaz M and Cleries R: Primary liver cancer: worldwide incidence and trends. Gastroenterology 127: S5-S16, 2004.
11. Hamasaki K, Nakata K, Tsutsumi T, *et al*: Changes in the prevalence of hepatitis B and C infection in patients with hepatocellular carcinoma in the Nagasaki Prefecture, Japan. J Med Virol 40: 146-149, 1993.
12. Kato Y, Nakata K, Omagari K, *et al*: Risk of hepatocellular carcinoma in patients with cirrhosis in Japan. Analysis of infectious hepatitis viruses. Cancer 74: 2234-2238, 1994.
13. Shiratori Y, Shiina S, Imamura M, *et al*: Characteristic difference of hepatocellular carcinoma between hepatitis B- and C- viral infection in Japan. Hepatology 22: 1027-1033, 1995.
14. Shiratori Y, Shiina S, Zhang PY, *et al*: Does dual infection by hepatitis B and C viruses play an important role in the pathogenesis of hepatocellular carcinoma in Japan? Cancer 80: 2060-2067, 1997.
15. Kiyosawa K, Umemura T, Ichijo T, *et al*: Hepatocellular carcinoma: recent trends in Japan. Gastroenterology 127: S17-S26, 2004.
16. Yoshizawa H: Hepatocellular carcinoma associated with hepatitis C virus infection in Japan: projection to other countries in the foreseeable future. Oncology 62: 8-17, 2002.
17. Umemura T and Kiyosawa K: Epidemiology of hepatocellular carcinoma in Japan. Hepatol Res 37 (Suppl 2): S95-S100, 2007.
18. Taura N, Yatsuhashi H, Hamasaki K, *et al*: Increasing hepatitis C virus-associated hepatocellular carcinoma mortality and aging: Long term trends in Japan. Hepatol Res 34: 130-134, 2006.
19. Taura N, Hamasaki K, Nakao K, *et al*: Aging of patients with hepatitis C virus-associated hepatocellular carcinoma: long-term trends in Japan. Oncol Rep 16: 837-843, 2006.
20. Nishiguchi S, Kuroki T, Nakatani S, *et al*: Randomised trial of effects of interferon-alpha on incidence of hepatocellular carcinoma in chronic active hepatitis C with cirrhosis. Lancet 346: 1051-1055, 1995.
21. Nishiguchi S, Shiomi S, Nakatani S, *et al*: Prevention of hepatocellular carcinoma in patients with chronic active hepatitis C and cirrhosis. Lancet 357: 196-197, 2001.
22. Kasahara A, Hayashi N, Mochizuki K, *et al*: Risk factors for hepatocellular carcinoma and its incidence after interferon treatment in patients with chronic hepatitis C. Osaka Liver Disease Study Group. Hepatology 27: 1394-1402, 1998.
23. Ikeda K, Saitoh S, Arase Y, *et al*: Effect of interferon therapy on hepatocellular carcinogenesis in patients with chronic hepatitis type C: A long-term observation study of 1,643 patients using statistical bias correction with proportional hazard analysis. Hepatology 29: 1124-1130, 1999.
24. Makiyama A, Itoh Y, Kasahara A, *et al*: Characteristics of patients with chronic hepatitis C who develop hepatocellular carcinoma after a sustained response to interferon therapy. Cancer 101: 1616-1622, 2004.
25. Kato J, Miyanishi K, Kobune M, *et al*: Long-term phlebotomy with low-iron diet therapy lowers risk of development of hepatocellular carcinoma from chronic hepatitis C. J Gastroenterol 42: 830-836, 2007.
26. Furutani T, Hino K, Okuda M, *et al*: Hepatic iron overload induces hepatocellular carcinoma in transgenic mice expressing the hepatitis C virus polyprotein. Gastroenterology 130: 2087-2098, 2006.
27. Muto Y, Sato S, Watanabe A, *et al*: Effects of oral branched-chain amino acid granules on event-free survival in patients with liver cirrhosis. Clin Gastroenterol Hepatol 3: 705-713, 2005.
28. Deuffic S, Poynard T and Valleron AJ: Correlation between hepatitis C virus prevalence and hepatocellular carcinoma mortality in Europe. J Viral Hepat 6: 411-413, 1999.
29. El-Serag HB and Mason AC: Rising incidence of hepatocellular carcinoma in the United States. N Engl J Med 340: 745-750, 1999.
30. Planas R, Balleste B, Antonio Alvarez M, *et al*: Natural history of decompensated hepatitis C virus-related cirrhosis. A study of 200 patients. J Hepatol 40: 823-830, 2004.
31. Davila JA, Morgan RO, Shaib Y, McGlynn KA and El-Serag HB: Hepatitis C infection and the increasing incidence of hepatocellular carcinoma: a population-based study. Gastroenterology 127: 1372-1380, 2004.
32. Sasaki F, Tanaka J, Moriya T, *et al*: Very low incidence rates of community-acquired hepatitis C virus infection in company employees, long-term inpatients, and blood donors in Japan. J Epidemiol 6: 198-203, 1996.

The Polycomb Gene Product BMI1 Contributes to the Maintenance of Tumor-Initiating Side Population Cells in Hepatocellular Carcinoma

Tetsuhiro Chiba,[1,4] Satoru Miyagi,[1] Atsunori Saraya,[1] Ryutaro Aoki,[1] Atsuyoshi Seki,[1] Yohei Morita,[3] Yutaka Yonemitsu,[2] Osamu Yokosuka,[2] Hideki Taniguchi,[5] Hiromitsu Nakauchi,[3] and Atsushi Iwama[1,4]

[1]Department of Cellular and Molecular Medicine and [2]Department of Medicine and Clinical Oncology, Graduate School of Medicine, Chiba University, Chiba, Japan; [3]Laboratory of Stem Cell Therapy, Center for Experimental Medicine, University of Tokyo; [4]JST, CREST, Tokyo, Japan; and [5]Department of Regenerative Medicine, Graduate School of Medical Science, Yokohama City University, Yokohama, Japan

Abstract

Side population (SP) cell analysis and sorting have been successfully applied to hepatocellular carcinoma (HCC) cell lines to identify a minor cell population with cancer stem cell properties. However, the molecular mechanisms operating in SP cells remain unclear. The polycomb gene product BMI1 plays a central role in the self-renewal of somatic stem cells in a variety of tissues and organs and seems to be implicated in tumor development. In this study, we determined the critical role of BMI1 in the maintenance of cancer stem cells with the SP phenotype in HCC cell lines. BMI1 was preferentially expressed in SP cells in Huh7 and PLC/PRF/5 HCC cells compared with the corresponding non-SP cells. Lentiviral knockdown of *BMI1* considerably decreased the number of SP cells in both Huh7 and PLC/PRF/5 cells. Long-term culture of purified SP cells resulted in a drastic reduction in the SP subpopulation upon the *BMI1* knockdown, indicating that BMI1 is required for the self-renewal of SP cells in culture. More importantly, the *BMI1* knockdown abolished the tumor-initiating ability of SP cells in nonobese diabetic/severe combined immunodeficiency mice. Derepression of the *INK4A* and *ARF* genes that are major targets for BMI1 was not necessarily associated with impaired self-renewal of SP cells caused by *BMI1* knockdown. In conclusion, our findings define an important role for BMI1 in the maintenance of tumor-initiating SP cells in HCC. BMI1 might be a novel therapeutic target for the eradication of cancer stem cells in HCC. [Cancer Res 2008;68(19):7742–9]

Introduction

According to the recent "cancer stem cell hypothesis," tumors consist of a minor component of tumorigenic cells and a major component of nontumorigenic cells (1, 2). The minor population, termed cancer stem cells or tumor-initiating cells, construct a hierarchical structure containing varied descendants in a similar fashion to the normal stem cell systems and possesses a prominent ability to initiate new tumors in xenograft transplantation (3, 4). In addition, these cells seem to be highly resistant to traditional forms of anticancer therapy such as chemotherapy and radiotherapy (5, 6), resulting in residual cancer stem cells which, in many instances, lead to the recurrence of the cancer (7). Therefore, an overall understanding of the various biological aspects of cancer stem cells is of paramount importance to both the elucidation of mechanisms underlying carcinogenesis and the establishment of novel therapeutic strategies.

Side population (SP) cell analysis and sorting were initially used for the isolation of hematopoietic stem cells in bone marrow cells (8). Currently, they are widely applied to the enrichment of putative normal stem cells in a variety of tissues and organs (9–11). The SP phenotype is determined by the ability to efflux the Hoechst 33342 dye through an ATP-binding cassette (ABC) membrane transporter. Of note, recent studies showed that SP cells isolated from diverse cancer cell lines harbor stem cell–like properties (12–14). Given that many different types of cancer cells frequently show overexpression of ABC transporters and exhibit drug resistance (15), it is quite reasonable to detect stem-like fractions in cancer cells using this approach. We previously applied SP analysis and sorting to established hepatocellular carcinoma (HCC) cell lines and found that in Huh7 and PLC/PRF/5 cells, SP fractions made up <1% of the total cell population (12). As expected, the SP subpopulations showed cancer stem cell–like properties both in culture and in an *in vivo* transplant model. These stem cell biology-based strategies enabled us to perform further analyses.

We and others previously reported that the polycomb-group (PcG) gene *Bmi1* plays a critical role in the self-renewal of a range of somatic stem cells, including hepatic stem cells, based on gain-of-function and loss-of-function analyses (16, 17). It seems likely that both normal and cancer stem cells share not only a number of surface marker phenotypes but also a list of molecular mechanisms for self-renewal and differentiation. This has been well shown in the leukemic stem cell system (18–20), although little is known in solid cancers.

In the current study, we examined the crucial role of BMI1 in the maintenance of the tumor-initiating SP subpopulation in HCC cells. Taking advantage of lentivirus-mediated knockdown and retrovirus-mediated overexpression techniques, we examined whether BMI1 regulates the self-renewal and differentiation of SP cells in culture and their tumorigenicity in a nonobese diabetic/severe combined immunodeficient (NOD/SCID) xenograft transplant model.

Note: Supplementary data for this article are available at Cancer Research Online (http://cancerres.aacrjournals.org/).

Requests for reprints: Atsushi Iwama, Department of Cellular and Molecular Medicine, Graduate School of Medicine, Chiba University, 1-8-1 Inohana, Chu-ku, Chiba 260-8670, Japan. Phone: 81-43-2262189; Fax: 81-43-2262191; E-mail: aiwama@faculty.chiba-u.jp.

doi:10.1158/0008-5472.CAN-07-5882

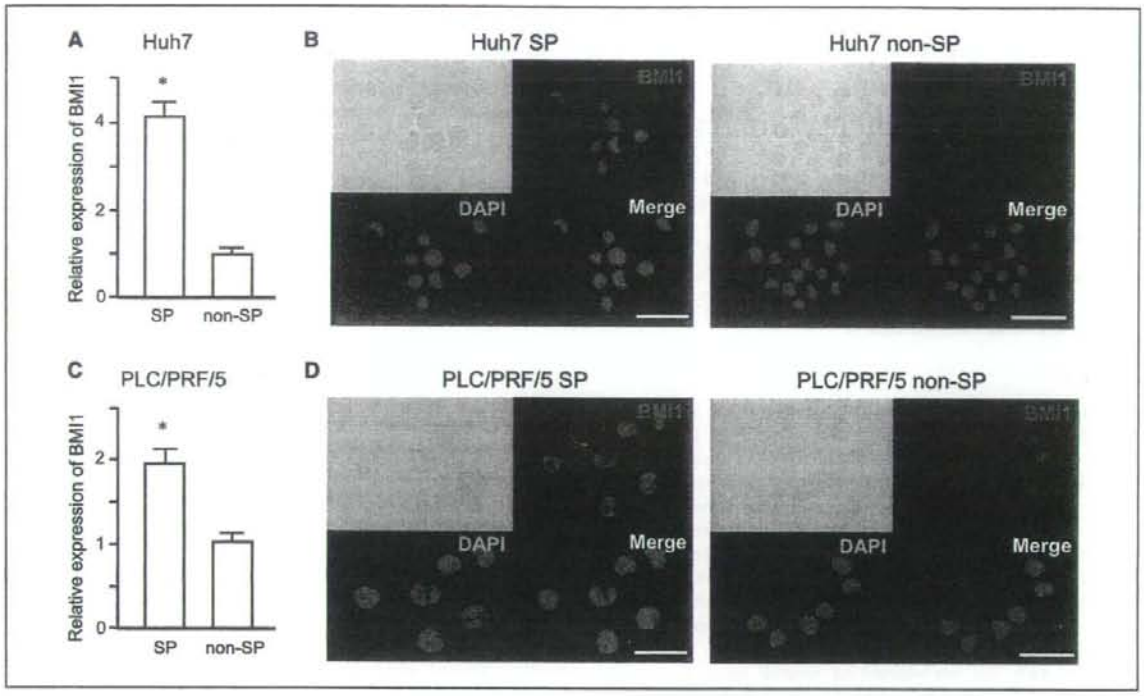

Figure 1. Expression of BMI1 in SP and non-SP cells. Real-time RT-PCR analyses of *BMI1* expression in SP and non-SP cells from Huh7 (*A*) and PLC/PRF/5 cells (*C*). Immunocytochemical analyses of BMI1 expression in SP and non-SP cells from Huh7 (*B*) and PLC/PRF/5 cells (*D*). Nuclear DAPI staining (*blue*) and immunofluorescent labeling of BMI1 (*red*) are merged. *, statistically significant ($P < 0.05$). *Scale bar*, 50 μm.

Materials and Methods

Mice. NOD/SCID mice were purchased from Sankyo Laboratory Co. Ltd. They were bred and maintained in accordance with our institutional guidelines for the use of laboratory animals.

Cell culture. The human liver cancer cell lines Huh7 and PLC/PRF/5 were cultured in DMEM (Invitrogen Life Technologies) containing 10% FCS and 1% penicillin/streptomycin (Invitrogen).

Flow cytometry. SP analysis and sorting were performed, as described previously (12). Briefly, the suspended cells were incubated at 37°C for 90 min with 20 μg/mL Hoechst 33342 (Sigma Chemical), either alone or in the presence of 50 μmol/L verapamil (Sigma). For the analysis of CD133 expression, cells were incubated with phycoerythrin-conjugated CD133/1 (Miltenyi Biotec). Propidium iodide (BD PharMingen) was added for the elimination of dead cells. Cell analysis and sorting were performed using MoFlo (DakoCytomation).

Immunocytochemistry. Freshly isolated SP cells and non-SP cells were placed on poly-L-lysine–coated slide glasses. After fixation with 2% paraformaldehyde and blocking in 10% goat serum, the cells were incubated with 0.5% Triton-X in PBS for 20 min at room temperature. After incubation, the cells were stained with a primary antibody, anti-Bmi1 (F6; Upstate Biotechnology), at a dilution of 1:200 for 12 h at 4°C. The cells then were washed and incubated with Alexa-555–conjugated goat anti-mouse IgG (Molecular Probes) at a dilution of 1:500 for 2 h at room temperature. After being washed in PBS, the cells were coverslipped with a mounting medium containing 4′,6-diamidino-2-phenylindole (DAPI; Vector Laboratories).

Viral production and transduction. Lentiviral vectors (CS-H1-shRNA-EF-1α-EGFP) expressing short hairpin RNA (shRNA) that targets human *BMI1* (target sequence: sh-*BMI1*-1, 5′-CAGATGAAGATAAGAGAAT-3′; sh-*BMI1*-2, 5′-GAGAAGGAATGGTCCACTT-3′) and *luciferase* were constructed. Human *BMI1* cDNA (a kind gift from Dr. Kazuhito Yamamoto) was cloned into a site upstream of IRES–enhanced green fluorescent protein (EGFP) in the pMCs-IG retroviral vector (21). Recombinant lentiviruses and retroviruses were produced as described before (17, 22).

Western blotting. Cells transduced with the indicated viruses were selected by cell sorting for EGFP expression and subjected to Western blot analysis using anti-Bmi1 (F6) and anti–α-tubulin (Ab-1; Oncogene Science) antibodies.

Reverse transcription–PCR. Total RNA extraction and cDNA synthesis were conducted, as described previously (12). Real-time PCR was performed using TaqMan technology and the ABI PRISM 7000 Sequence Detection System (Applied Biosystems). TaqMan probe and primers for *BMI1* (assay ID Hs00180411_m1) and *β-actin* (assay ID Hs99999903_m1) were obtained from TaqMan gene expression assays (Applied Biosystems). To examine the mRNA expression of *INK4A/ARF* genes in SP cells following *BMI1* knockdown, multiplex reverse transcription–PCR (RT-PCR) was performed as described previously (23). PCR for *BMI1* and *β-actin* was conducted using the following primers: *BMI1* (forward 5′-AGC AGC AAT GAC TGT GAT GC-3′, reverse 5′-CAG TCT CAG GTA TCA ACC AG-3′), *β-actin* (forward 5′-ATC CTG CGT CTG GAC CTG GCT GG-3′, reverse 5′-ACA TGC CGG AGC CGT TGT CGA CGA-3′).

Xenograft transplantation. Various numbers of SP and non-SP cells stably expressing shRNA against *BMI1* or *luciferase* were suspended in DMEM and Matrigel (Becton Dickinson; 1:1) and transplanted to NOD/SCID mice (male, 6–10 wk) under anesthesia. *BMI1* knockdown cells and control cells were implanted into the s.c. space on the right and left sides of the back of recipient mice, respectively. To examine whether enforced expression of *BMI1* in SP cells promotes tumorigenesis, 1×10^4 Huh7 SP cells transduced with *BMI1* and *EGFP* retroviruses were also transplanted.

Tumor formation was observed weekly for 14 wk. The transplantation assays were performed in accordance with institutional guidelines for the use of laboratory animals.

Immunohistochemical analysis. The subcutaneous tumors formed in NOD/SCID mice were fixed in formalin and embedded in paraffin. The sections were subjected to H&E staining. For dual immunohistochemical analyses, the sections were stained with anti-EGFP (BD Biosciences Clontech) and anti-BMI1 (F6), followed by incubation with Alexa-488–conjugated goat anti-rabbit IgG and Alexa-555–conjugated goat anti-mouse IgG (Molecular Probes), respectively.

Statistical analysis. Data are presented as the means ± SE. Statistical differences between two groups were analyzed using the Mann-Whitney units test. P values <0.05 were considered significant.

Results

Preferential expression of BMI1 in SP cells. To gain insight into the crucial role of the polycomb gene product BMI1, we first examined the basal expression of BMI1 in the SP population in Huh7 and PLC/PRF/5 cells. Real-time RT-PCR analyses showed that the mRNA expression of *BMI1* was 4.10 ± 0.36-fold and 1.92 ± 0.25-fold higher in Huh7 and PLC/PRF/5 SP cells than in the corresponding non-SP cells, respectively (Fig. 1*A* and *C*). Immunocytochemical analyses confirmed that BMI1 is highly expressed in the nuclei of SP cells rather than the corresponding non-SP cells in both cell lines (Fig. 1*B* and *D*).

Stable knockdown of *BMI1* by shRNA. We next performed loss-of-function analyses of BMI1 *in vitro*. Stable knockdown of *BMI1* in Huh7 and PLC/PRF/5 cells was achieved by lentivirus-mediated delivery of shRNA against *BMI1*. A lentiviral vector expressing shRNA against *luciferase* was used as a control. We obtained stable cell lines expressing shRNA against *BMI1* or *luciferase* by cell sorting using EGFP as a marker for infection. Western blot analysis showed that both sh-*BMI1*-1 and sh-*BMI1*-2 markedly repressed BMI1 expression in both cell lines, although sh-*BMI1*-1 was less effective than sh-*BMI1*-2 (Fig. 2*A*). Both shRNA inhibited the growth of HCC cell lines. In good agreement with the Western blot data, sh-*BMI1*-2 was more effective in growth suppression than sh-*BMI1*-1 (Fig. 2*B* and *C*). The viability of cells expressing shRNA against *BMI1* was comparable with that of control cells (data not shown).

Detection and isolation of SP cells. SP cell analysis and sorting were performed in Huh7 and PLC/PRF/5 cells stably expressing shRNA against *BMI1* (Fig. 3 and Supplementary Fig. S1). *BMI1* knockdown using sh-*BMI1*-2 considerably decreased the size of the SP population from 0.67 ± 0.09% to 0.19 ± 0.03% in Huh7 cells and from 0.87 ± 0.10% to 0.40 ± 0.04% in PLC/PRF/5 cells (Fig. 3). On the other hand, *BMI1* knockdown using sh-*BMI1*-1 slightly decreased the percentage of SP cells from 0.59 ± 0.04% to 0.32 ± 0.03% in Huh7 cells and from 0.82 ± 0.06% to 0.47 ± 0.03% in PLC/PRF/5 cells (Supplementary Fig. S1). The SP population showed a drastic reduction in number on treatment with the calcium channel blocker verapamil.

Stable overexpression of *BMI1* by retroviral vector. Next, we tested the overexpression of *BMI1* in HCC cells (Supplementary Fig. S2*A*). In clear contrast with the knockdown experiment, the SP subpopulation increased nearly 8-fold with the overexpression of *BMI1* in Huh7 cells (Supplementary Fig. S2*B*). Next, we examined the tumorigenicity of Huh7 SP cells transduced with *BMI1* in NOD/SCID xenograft transplantation. The implantation of 1×10^4 SP cells transduced with *BMI1* resulted in early onset and aggressive

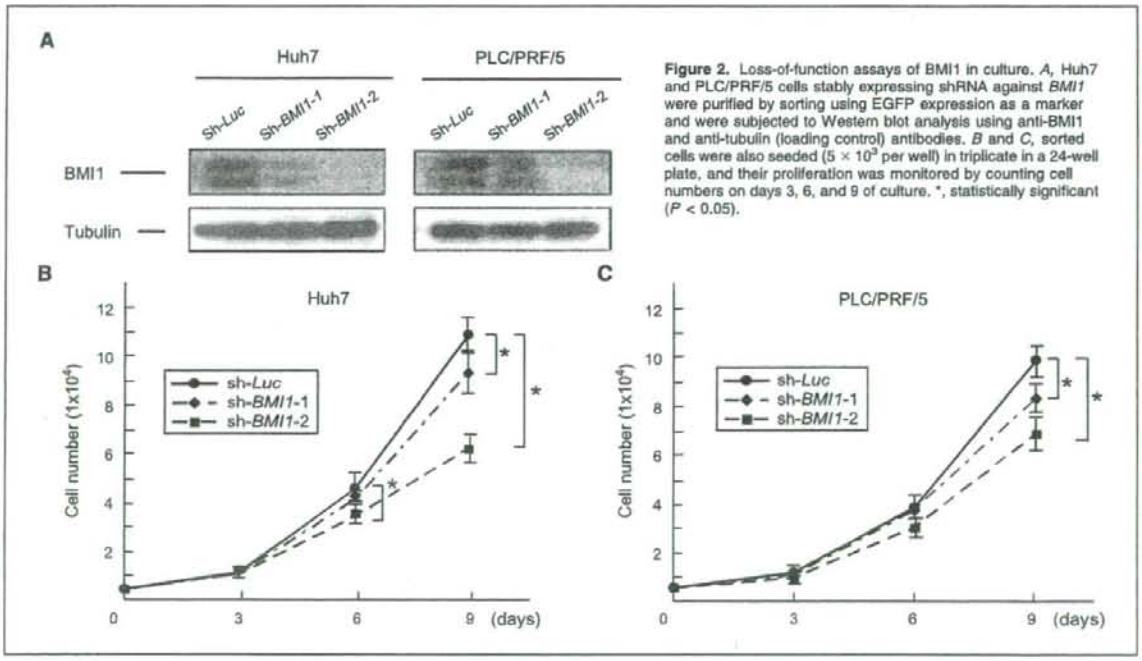

Figure 2. Loss-of-function assays of BMI1 in culture. *A*, Huh7 and PLC/PRF/5 cells stably expressing shRNA against *BMI1* were purified by sorting using EGFP expression as a marker and were subjected to Western blot analysis using anti-BMI1 and anti-tubulin (loading control) antibodies. *B* and *C*, sorted cells were also seeded (5×10^3 per well) in triplicate in a 24-well plate, and their proliferation was monitored by counting cell numbers on days 3, 6, and 9 of culture. *, statistically significant ($P < 0.05$).

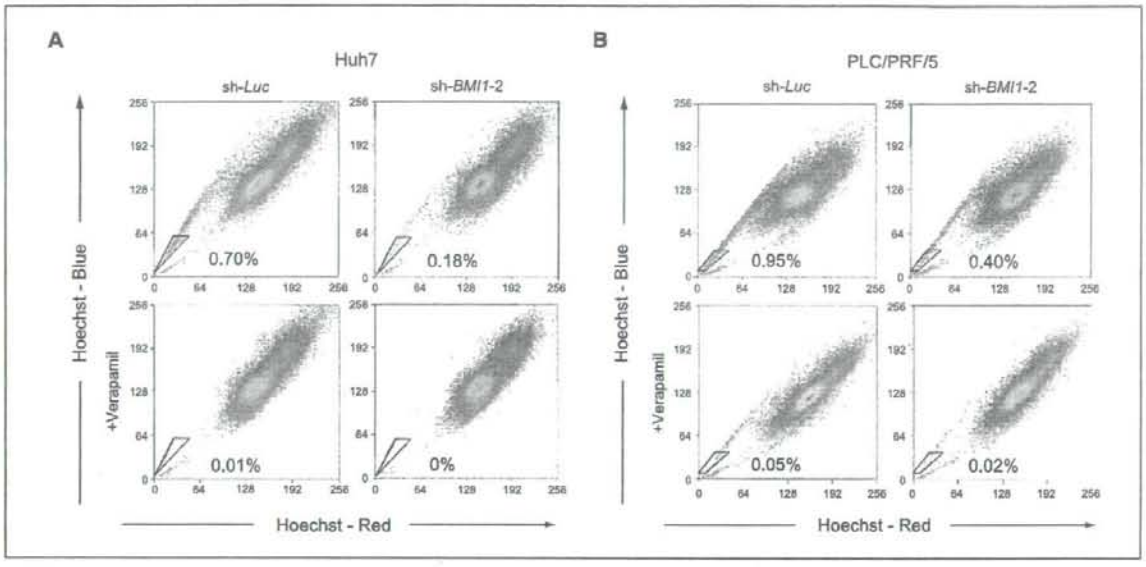

Figure 3. SP cell analysis in *BMI1* knockdown HCC cells by sh-*BMI1*-2. Flow cytometric profiles of SP cells among Huh7 (*A*) and PLC/PRF/5 cells (*B*) after stable knockdown of *BMI1* by sh-*BMI1*-2. SP cell profiles in the presence of verapamil are depicted at the bottom. The percentages of SP cells are indicated.

tumor growth compared with that of control SP cells expressing EGFP (Supplementary Fig. S2*C* and *D*). These results indicated that forced expression of *BMI1* leads to not only enhanced self-renewal but also increased tumorigenicity of SP cells.

Expression of the *INK4A/ARF* gene in *BMI1* knockdown SP cells. To address whether the knockdown of *BMI1* causes derepression of the *INK4A* and *ARF* genes as observed in *Bmi1*-deficient hematopoietic stem cells (HSC; ref. 17), we examined their mRNA expression in SP cells freshly isolated from *BMI1* knockdown and control cells (Fig. 4*A*). In Huh7 SP cells, in which *INK4A* expression is repressed by aberrant DNA methylation in its promoter region (23) and *ARF* is constitutively expressed, *BMI1* knockdown did not affect their expression at all. Conversely, *BMI1* knockdown in PLC/PRF/5 SP cells, in which both *INK4A* and *ARF* are moderately expressed, greatly augmented their expression.

Reanalysis of isolated SP cells. We have previously reported that purified SP cells self-renew and generate nontumorigenic non-SP cells through asymmetrical cell division *in vivo* (12). Purified SP cells repopulate the same hierarchical structure as the original tumor cells consisting of a minor component of SP cells and a major component of non-SP cells (12, 24). This process occurs both *in vitro* and *in vivo*. The SP cells in repopulated tumor retain the same tumor-initiating capacity as the original SP cells. We purified SP cells from both *BMI1* knockdown and control cells and cultured them for 4 weeks to examine the role of BMI1 in this process in culture. The SP subpopulation in *BMI1* knockdown Huh7 cells profoundly decreased (5.5%) compared with that in the control cells (18.8%; Fig. 4*B*). Likewise, the percentage of PLC/PRF/5 SP cells among *BMI1* knockdown and control cells was 6.1% and 22.0%, respectively (Fig. 4*B*). These results imply that BMI1 regulates the self-renewal capability of tumor-initiating SP cells and loss of BMI1 accelerates differentiation toward nontumorigenic non-SP cells.

The role for BMI1 in the maintenance of tumorigenic CD133-positive Huh7 cells. It has been reported that CD133-positive cells possessed greater tumorigenicity than CD133-negative cells in HCC cells, including Huh7 cells (25). Although the majority of Huh7 cells are CD133-positive (Fig. 4*C*), it has been shown that CD133 expression is stronger in SP cells than in non-SP cells (24). We then evaluated the expression of CD133 in the context of BMI1 expression using flow cytometry. *BMI1* knockdown decreased the CD133-positive fraction from 74.2% to 60.9%, whereas *BMI1* overexpression increased it from 71.6% to 84.4% (Fig. 4*C*). These findings indicate that the expression level of BMI1 is tightly correlated with the cancer stem cell phenotype represented not only by SP cells but also by CD133-positive cells.

Tumorigenic ability in xenograft transplantation. To determine whether loss of BMI1 affects the tumorigenicity *in vivo*, various numbers of SP and non-SP cells sorted from the *BMI1* knockdown or control HCC cells were transplanted into NOD/SCID mice (Fig. 5; Table 1). As few as 1×10^3 control SP cells were enough to initiate tumors for both cell lines. In contrast, 1×10^3 *BMI1* knockdown SP cells transduced with sh-*BMI1*-1 and 1×10^4 *BMI1* knockdown SP cells transduced with sh-*BMI1*-2 from Huh7 and PLC/PRF/5 cells failed to initiate subcutaneous tumors in any recipient mice. Tumors derived from control SP cells showed similar histologic features to those formed by the injection of unsorted cells and exhibited the nuclear expression of BMI1 (Fig. 5). Unexpectedly, 1×10^5 *BMI1* knockdown Huh7 and PLC/PRF/5 SP cells with sh-*BMI1*-2 gave rise to tumors in one of three and one of two mice, respectively. However, the tumor size was less than half that of control SP cells. Furthermore,

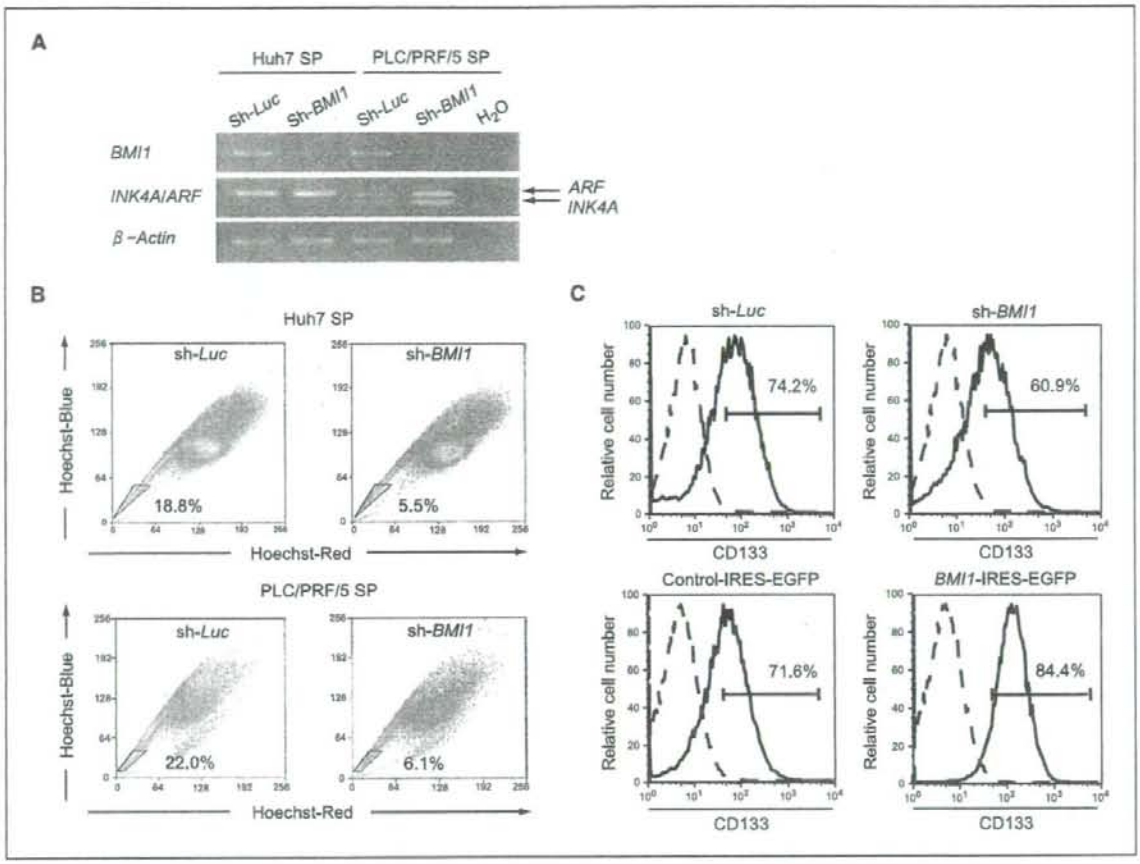

Figure 4. Role of BMI1 in *INK4A/ARF* expression and cancer stem cell phenotype. *A*, RT-PCR analysis of *INK4A/ARF* in *BMI1* knockdown SP cells from Huh7 and PLC/PRF/5 cells. Lane H_2O represents the negative control without the template. *B*, flow cytometric profiles of purified SP cells after culture. SP cells were purified from *BMI1* knockdown cells, cultured for 4 wk, and then subjected to the flow cytometric analysis. *C*, expression of CD133 in *BMI1* knockdown (*top*) and *BMI1* overexpressing cells (*bottom*) detected by flow cytometric analysis. Dotted line represents negative controls. The percentages of CD133-positive cells are indicated.

immunohistochemical analyses revealed that tumors predominantly consisted of contaminating EGFP-negative cells or EGFP-positive cells showing no obvious effects of *BMI1* knockdown (Supplementary Fig. S3). By contrast, tumors derived from control SP cells did not contain EGFP-negative cells at all (Fig. 5). These results further support that the tumor-initiating capacity is profoundly impaired by *BMI1* knockdown. In contrast, the injection of 1×10^6 non-SP cells from either cell line failed to generate tumors in any mice.

Discussion

PcG proteins form chromatin-associated multiprotein complexes, polycomb repressive complex 1 (PRC1) and PRC2 and function as a cellular memory system through epigenetic chromatin modifications (26, 27). Bmi1, a component of PRC1, has been implicated in the regulation of self-renewal in a range of different stem cell systems (28, 29). Of note, Bmi1 is also required for the maintenance of self-renewing leukemic stem cells in a mouse model using *Bmi1*$^{-/-}$ HSCs (30). Recent reports described that BMI1 is preferentially expressed in the tumorigenic subpopulation in breast cancer and head and neck tumors (31, 32). Consistent with these reports, we previously showed that forced expression of *BMI1* promotes the self-renewal of hepatic stem/progenitor cells and contributes to malignant transformation (16). In addition, immunohistochemical analyses showed BMI1 to be overexpressed in >60% of human HCC cases examined.[6] Together, all these findings highlight the importance of BMI1 in hepatocarcinogenesis and implicate BMI1 in the self-renewal of cancer stem cells in HCC.

In the present study, we first examined the basal expression of BMI1 in Huh7 and PLC/PRF/5 SP cells. As expected, both the real-

[6] Unpublished data.

time RT-PCR and immunocytochemical analyses showed BMI1 expression to be stronger in SP cells than non-SP cells in each cell line. We thus directly evaluated the role of BMI1 in cancer stem cell–like SP cells. Lentiviral shRNA-mediated knockdown of *BMI1* allowed a highly efficient loss-of-function assay of the SP subpopulation in culture and in an *in vivo* transplant model. The analysis showed a significant decrease in the frequency of SP cells among the *BMI1* knockdown cells compared with the corresponding control cells. Furthermore, analysis of the growth and differentiation of purified SP cells revealed that loss of BMI1 causes a considerable decrease in the SP subpopulation and facilitates differentiation toward non-SP cells. These results indicated that BMI1 contributes to the self-renewal of SP cells in culture.

Notably, when as few as 1×10^3 control SP cells were sufficient to initiate tumors in NOD/SCID mice, even 10 times more *BMI1* knockdown SP cells (1×10^4) failed to develop tumors. 1×10^5 *BMI1* knockdown SP cells gave increase to tumors in some of the recipient mice, but the tumor-initiating capacity was profoundly reduced. Collectively, the tumorigenic activity in the SP subpopulation seemed to be attenuated nearly 100-fold by the *BMI1* knockdown. Although the important role of Bmi1 in the maintenance of cancer stem cells has already been shown in a mouse leukemia model, this is the first direct evidence that the loss of BMI1 in established cancer stem cells can affect their ability to self-renew and tumorigenicity. The role of BMI1 in the regulation of tumor-initiating SP cells was further supported by the findings of the gain-of-function assay. Although stable knockdown of *BMI1* decreased SP cell numbers *in vitro*, it did not completely abolish SP cells and its effect varied among HCC cell lines. These results strongly indicate that the SP subpopulation is quite heterogeneous, and the contribution of BMI1 to the SP phenotype differs among the cell lines. Considering that BMI1 is just one of multiple self-renewal regulators, the different contributions of molecular machinery, including the Notch, Wnt, and Shh signaling pathways, might also influence the SP phenotype (33). Further analyses would be necessary to clarify the mechanisms underlying the regulation of cancer stem cells in HCC.

Bmi1 regulates the cell cycle, apoptosis and senescence by repressing the *Ink4a/Arf* locus (26, 34). In *Bmi1*-deficient mice, the expression of *Ink4a* and *Arf* is markedly increased in HSCs (17). Conversely, deletion of both *Ink4a* and *Arf* substantially restores the impaired capacity of *Bmi1*$^{-/-}$ HSCs to self-renew (22). These findings suggest that Bmi1 regulates HSCs by acting as a critical failsafe against the premature loss of HSCs induced by Ink4a and Arf-dependent senescence pathways. On the other hand, the Ink4a-Rb and Arf-p53–dependent cellular senescence pathways play a critical role in the triggering of oncogene-induced senescence, which is of substantial importance to the elimination of transforming cells that potentially develop into cancer stem cells (26, 35). In the present study, the expression of the *INK4A* and *ARF* genes was augmented by *BMI1* knockdown in PLC/PRF/5 cells. In this case, derepression of *INK4A* and *ARF* could account for the impaired self-renewal of PLC/PRF/5 SP cells with *BMI1* knockdown. On the other hand, knockdown of *BMI1* in Huh7 cells resulted in no remarkable changes in *INK4A* and *ARF* gene expression compared with the control. Given that the function of p53 is impeded by mutations in Huh7 cells (36), additional targets for BMI1 other than the *INK4A/ARF* locus might be responsible for

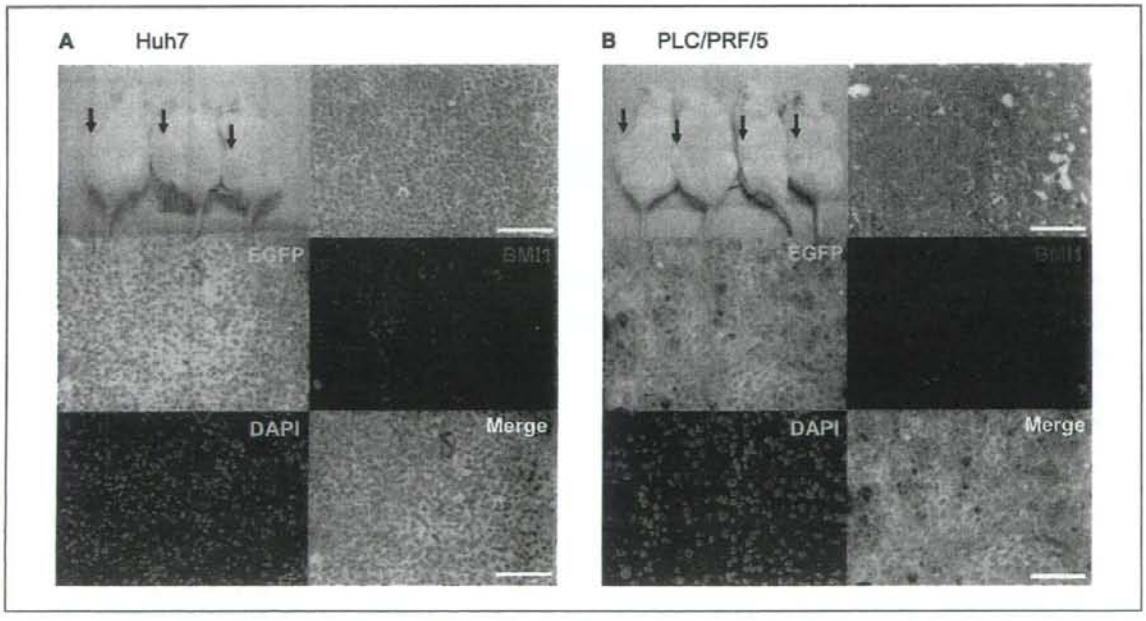

Figure 5. Loss of tumorigenicity in SP cells by *BMI1* knockdown. 1×10^3 control SP cells from Huh7 (*A*) and PLC/PRF/5 cells (*B*) generated tumors in the left subcutaneous space of recipient mice (*arrows*), whereas *BMI1* knockdown SP cells failed to initiate tumors in the right space. Immunohistochemical analyses revealed the nuclear localization of BMI1 in tumor cells generated by control SP cells. *Scale bar*, 100 μm.

Table 1. Tumor-initiating ability of SP cells in the NOD/SCID xenograft transplant model

	No. implanted cells				
	100	1×10^3	1×10^4	1×10^5	1×10^6
Huh7					
sh-*Luc*					
SP cells	0/5	14/15	13/13		
Non-SP cells		0/15	0/14	0/10	0/5
sh-*BMI1*-1					
SP cells	0/5	0/6	3/6*		
Non-SP cells		0/6	0/6	0/5	0/5
sh-*BMI1*-2					
SP cells	0/5	0/9	0/8	1/3†	
Non-SP cells		0/9	0/8	0/5	0/5
PLC/PRF/5					
Sh-*Luc*					
SP cells	0/5	14/14	14/14		
Non-SP cells		0/14	0/14	0/10	0/5
sh-*BMI1*-1					
SP cells	0/5	0/5	2/5*		
Non-SP cells		0/4	0/5	0/5	0/5
sh-*BMI1*-2					
SP cells	0/5	0/9	0/9	1/2†	
Non-SP cells		0/9	0/9	0/5	0/5

NOTE: Tumor initiation was monitored for 14 wk after implantation.
*Delayed tumor formation and a decrease in tumor size were observed compared with tumors derived from control SP cells.
†Immunohistochemical data for tumors are displayed in Supplementary Fig. S3.

the impaired ability of Huh7 SP cells to self-renew. Thus, BMI1 might function in the maintenance of HCC cancer stem cells in both an *INK4A/ARF*-dependent and an *INK4A/ARF*-independent manner.

Finally, the present loss-of-function and gain-of-function assays revealed that BMI1 determines the self-renewal capability of SP cells, which directly contributes to the tumorigenic potential. However, further analysis will definitely be necessary to determine the role of BMI1 in primary HCC cancer stem cells (37). Our findings also indicate BMI1 to be a novel therapeutic target for the eradication of cancer stem cells in HCC. It would be of paramount importance to understand differential functions and targets of BMI1 in normal and cancer stem cells.

Disclosure of Potential Conflicts of Interest

No potential conflicts of interest were disclosed.

Acknowledgments

Received 10/15/2007; revised 7/10/2008; accepted 7/18/2008.

Grant support: Ministry of Education, Culture, Sports, Science and Technology, Japan; Core Research for Evolutional Science and Technology of Japan Science and Technology Corporation; and the Public Trust Haraguchi Memorial Cancer Research Fund and Sagawa Foundation for Promotion for Cancer Research.

The costs of publication of this article were defrayed in part by the payment of page charges. This article must therefore be hereby marked *advertisement* in accordance with 18 U.S.C. Section 1734 solely to indicate this fact.

We thank Drs. Toshio Kitamura (Tokyo University) and Hiroyuki Miyoshi (RIKEN) for providing pMCs-IG and CS-H1-shRNA-EF-1α-EGFP, respectively, Yuji Yamazaki for technical support in flow cytometry and Mieko Tanemura for laboratory assistance.

References

1. Reya T, Morrison SJ, Clarke MF, Weissman IL. Stem cells, cancer, and cancer stem cells. Nature 2001;414:105–11.
2. Jordan CT, Guzman ML, Noble M. Cancer stem cells. N Engl J Med 2006;355:1253–61.
3. Bonnet D, Dick JE. Human acute myeloid leukemia is organized as a hierarchy that originates from a primitive hematopoietic cell. Nat Med 1997;3:730–7.
4. Al-Hajj M, Wicha MS, Benito-Hernandez A, Morrison SJ, Clarke MF. Prospective identification of tumorigenic breast cancer cells. Proc Natl Acad Sci U S A 2003;100:3983–8.
5. Dean M, Fojo T, Bates S. Tumour stem cells and drug resistance. Nat Rev Cancer 2005;5:275–84.
6. Bao S, Wu Q, McLendon RE, et al. Glioma stem cells promote radioresistance by preferential activation of the DNA damage response. Nature 2006;444:756–60.
7. Abraham BK, Fritz P, McClellan M, Hauptvogel P, Athelogou M, Brauch H. Prevalence of CD44+/CD24-/low cells in breast cancer may not be associated with clinical outcome but may favor distant metastasis. Clin Cancer Res 2005;11:1154–9.
8. Goodell MA, Brose K, Paradis G, Conner AS, Mulligan RC. Isolation and functional properties of murine hematopoietic stem cells that are replicating *in vivo*. J Exp Med 1996;183:1797–806.
9. Shimano K, Satake M, Okaya A, et al. Hepatic oval cells have the side population phenotype defined by expression of ATP-binding cassette transporter ABCG2/BCRP1. Am J Pathol 2003;163:3–9.
10. Falciatori I, Borsellino G, Haliassos N, et al. Identification and enrichment of spermatogonial stem cells displaying side-population phenotype in immature mouse testis. FASEB J 2004;18:376–8.
11. Asakura A, Seale P, Girgis-Gabardo A, Rudnicki MA. Myogenic specification of side population cells in skeletal muscle. J Cell Biol 2002;159:123–34.
12. Chiba T, Kita K, Zheng YW, et al. Side population purified from hepatocellular carcinoma cells harbors cancer stem cell-like properties. Hepatology 2006;44:240–51.
13. Kondo T, Setoguchi T, Taga T. Persistence of a small subpopulation of cancer stem-like cells in the C6 glioma cell line. Proc Natl Acad Sci U S A 2004;101:781–6.
14. Patrawala L, Calhoun T, Schneider-Broussard R, Zhou J, Claypool K, Tang DG. Side population is

enriched in tumorigenic, stem-like cancer cells, whereas ABCG2+ and ABCG2- cancer cells are similarly tumorigenic. Cancer Res 2005;65:6207–19.
15. Higgins CF. Multiple molecular mechanisms for multidrug resistance transporters. Nature 2007;446:749–57.
16. Chiba T, Zheng YW, Kita K, et al. Enhanced self-renewal capability in hepatic stem/progenitor cells drives cancer initiation. Gastroenterology 2007;133:937–50.
17. Iwama A, Oguro H, Negishi M, et al. Enhanced self-renewal of hematopoietic stem cells mediated by the polycomb gene product Bmi-1. Immunity 2004;21:843–51.
18. Lessard J, Sauvageau G. Polycomb group genes as epigenetic regulators of normal and leukemic hemopoiesis. Exp Hematol 2003;31:567–85.
19. Jamieson CH, Weissman IL, Passegue E. Chronic versus acute myelogenous leukemia: a question of self-renewal. Cancer Cell 2004;6:531–3.
20. Kato Y, Iwama A, Tadokoro Y, et al. Selective activation of STAT5 unveils its role in stem cell self-renewal in normal and leukemic hematopoiesis. J Exp Med 2005;202:169–79.
21. Kitamura T, Koshino Y, Shibata F, et al. Retrovirus-mediated gene transfer and expression cloning: powerful tools in functional genomics. Exp Hematol 2003;31:1007–14.
22. Oguro H, Iwama A, Morita Y, Kamijo T, van Lohuizen M, Nakauchi H. Differential impact of Ink4a and Arf on hematopoietic stem cells and their bone marrow microenvironment in Bmi1-deficient mice. J Exp Med 2006;203:2247–53.
23. Fukai K, Yokosuka O, Imazeki F, et al. Methylation status of p14ARF, p15INK4b, and p16INK4a genes in human hepatocellular carcinoma. Liver Int 2005;25:1209–16.
24. Haraguchi N, Utsunomiya T, Inoue H, et al. Characterization of a side population of cancer cells from human gastrointestinal system. Stem Cells 2006;24:506–13.
25. Ma S, Chan KW, Hu L, et al. Identification and characterization of tumorigenic liver cancer stem/progenitor cells. Gastroenterology 2007;132:5242–56.
26. Sparmann A, van Lohuizen M. Polycomb silencers control cell fate, development and cancer. Nat Rev Cancer 2006;6:846–56.
27. Valk-Lingbeek ME, Bruggeman SWM, van Lohuizen M. Stem cells and cancer: the polycomb connection. Cell 2004;118:409–18.
28. Park IK, Qian D, Kiel M, et al. Bmi-1 is required for maintenance of adult self-renewing haematopoietic stem cells. Nature 2003;423:302–5.
29. Molofsky AV, Pardal R, Iwashita T, Park IK, Clarke MF, Morrison SJ. Bmi-1 dependence distinguishes neural stem cell self-renewal from progenitor proliferation. Nature 2003;425:962–7.
30. Lessard J, Sauvageau G. Bmi-1 determines the proliferative capacity of normal and leukaemic stem cells. Nature 2003;423:255–60.
31. Liu S, Dontu G, Mantle ID, et al. Hedgehog signaling and Bmi-1 regulate self-renewal of normal and malignant human mammary stem cells. Cancer Res 2006;66:6063–71.
32. Prince ME, Sivanandan R, Kaczorowski A, et al. Identification of a subpopulation of cells with cancer stem cell properties in head and neck squamous cell carcinoma. Proc Natl Acad Sci U S A 2007;104:973–8.
33. Al-Hajj M, Clarke MF. Self-renewal and solid tumor stem cells. Oncogene 2004;23:7274–82.
34. Park IK, Morrison SJ, Clarke MF. Bmi1, stem cells, and senescence regulation. J Clin Invest 2004;113:175–9.
35. Collado M, Blasco MA, Serrano M. Cellular senescence in cancer and aging. Cell 2007;130:223–33.
36. Cagatay T, Ozturk M. P53 mutation as a source of aberrant β-catenin accumulation in cancer cells. Oncogene 2002;21:7971–80.
37. Yang ZF, Ho DW, Ng MN, et al. Significance of CD90+ cancer stem cells in human liver cancer. Cancer Cell 2008;13:153–66.

Liver International ISSN 1478-3223

CLINICAL STUDIES

Ultrasound-guided treatments under low acoustic power contrast harmonic imaging for hepatocellular carcinomas undetected by B-mode ultrasonography

Hitoshi Maruyama, Masanori Takahashi, Hiroyuki Ishibashi, Hidehiro Okugawa, Shinichiro Okabe, Masaharu Yoshikawa and Osamu Yokosuka

Department of Medicine and Clinical Oncology, Chiba University Graduate School of Medicine, Chiba, Japan

Keywords
contrast agent – hepatocellular carcinoma – liver – Sonazoid™ – ultrasound

Correspondence
Hitoshi Maruyama, Department of Medicine and Clinical Oncology, Chiba University Graduate School of Medicine, 1-8-1, Inohana, Chuou-ku, Chiba 260-8670, Japan
Tel: +81 43 2262083
Fax: +81 43 2262088
e-mail: maru-cib@umin.ac.jp

Received 9 June 2008
Accepted 26 July 2008

DOI:10.1111/j.1478-3231.2008.01875.x

Abstract

Background/Aims: The aim was to examine the efficacy of contrast-enhanced ultrasound (US) with Sonazoid™ to demonstrate ultrasonically unrecognizable hypervascular hepatocellular carcinoma (HCC) and apply percutaneous US-guided treatments. *Methods:* The subjects of this prospective study were 44 cirrhotic patients with 55 hypervascular lesions (12.7 ± 4.5 mm) found by contrast-enhanced computed tomography but unrecognized by non-contrast US. Contrast-enhanced US was performed to demonstrate these hepatic lesions after an intravenous injection of Sonazoid™ (0.0075 ml/kg). The sonograms in both the early phase (for 1 min after injection) and the late phase (5–10 min after) were taken in the harmonic imaging mode under a low mechanical index (0.24–0.3). *Results:* Fifty-three lesions were demonstrated by contrast-enhanced US, 52 with positive enhancement in the early phase and 44 with negative enhancement in the late phase. Percutaneous US-guided treatments were successfully performed for 42 lesions (ethanol injection in 20 and radiofrequency ablation in 22) in 32 patients with reference to contrast-enhanced US findings. Six patients were treated by transarterial chemoembolization alone because they had more than three lesions in the liver. In the remaining seven lesions in six patients, six were diagnosed as non-HCC lesions: five with vascular abnormalities such as arterioportal or arteriovenous communication and the other one with benign lesion in alcoholic liver disease. These six lesions and one HCC lesion with severe liver damage were followed up without any treatment. *Conclusions:* As the detectability of ultrasonically unrecognizable hypervascular HCC improved by contrast-enhanced US with Sonazoid™, a wider application of percutaneous US-guided treatments may be possible.

Hepatocellular carcinoma (HCC) is increasing worldwide and is one of the most common carcinomas in the eastern part of Asia (1). As the prognosis of cirrhotic patients depends on the occurrence and progression of HCC, management of this neoplasm is a major issue in clinical practice. However, surgical treatment is not always an appropriate choice, as the majority of HCC patients have poor liver function and recurrence is not rare (2–4).

Real-time observation is the most significant point to be emphasized in the clinical use of ultrasound (US), and the percutaneous US-guided technique is a reasonable procedure for the treatment of HCC with minimal invasiveness (5–9). Although these methods require demonstration of focal hepatic lesions by US, this is not always easy because of deformity and/or coarse parenchymal echo in cirrhotic liver, and modified echo patterns as a result of previous treatments (10, 11). Contrast-enhanced US with Levovist facilitated the application of percutaneous US-guided treatments by successful localization in about 75% of ultrasonically invisible hypervascular HCCs (12). However, the utility of second-generation microbubble contrast agents for the localization of such focal hepatic lesions has not been established.

Second-generation microbubble contrast agents have acquired stability of microbubble by homogenization of particle size distribution in comparison with

earlier agents (13, 14). The combination of second-generation contrast agents with harmonic imaging mode under lower mechanical index (MI) may provide US images with an improved signal-to-noise ratio, and a higher detection rate of focal lesions in the liver is expected (15, 16).

Sonazoid™ is a newly developed perflubutane US contrast agent (17–19). The microbubble has the characteristic property of accumulation in the Kupffer cell, and it is the largest difference between this agent and SonoVue, a popular agent in Europe. Application of Sonazoid-enhanced sonograms produced by accumulated microbubble as well as circulating microbubble may contribute greatly to the detection of focal hepatic lesions. With this background, the present study was designed to examine the efficacy of contrast-enhanced US with the new perflubutane microbubble agent Sonazoid™ in the visualization of ultrasonically unrecognized hepatic lesions that had a hypervascular appearance on contrast-enhanced computed tomography (CT), for the application of percutaneous US-guided treatments in cirrhotic patients.

Material and methods

Patients

Between February 2007 and May 2008, a prospective study was performed to examine the efficacy of contrast-enhanced US with Sonazoid™ (GE Healthcare, Oslo, Norway) to demonstrate hypervascular hepatic lesions seen on contrast-enhanced CT but not by non-contrast US in our department. The following criteria were used for study enrolment: (i) cirrhotic patients with solitary or multiple focal hypervascular lesions found by contrast-enhanced CT taken for the surveillance of HCC, (ii) radiological diagnosis of hepatic lesions was HCC on CT images, (iii) non-contrast US could not recognize the hepatic lesions and (iv) patients without egg allergy, a contraindication of Sonazoid™. In this study period, there were 1286 patients who received a contrast-enhanced CT examination for the surveillance of HCC in our department. Among them, the subjects of this study were 44 cirrhotic patients with 55 hypervascular lesions, and they consisted of 28 males and 16 females, aged 68.2 ± 9.2 years (range 33–78). The diagnosis of liver cirrhosis was based on imaging findings with clinical symptoms and biochemistry findings in all patients, with six patients positive for hepatitis B virus surface antigen, 33 positive for hepatitis C virus antibody, two with alcohol abuse and three patients cryptogenic. The total number of hypervascular lesions in all patients was 55 (one in 37 patients, two in four patients, three in two patients and four in one patients) with a size ranging from 5 to 24 mm (12.7 ± 4.5 mm) on CT images. The serum α-fetoprotein level ranged from 1.9 to 991.1 ng/ml, being normal in 20 patients and abnormal in 24 patients (109.6 ± 209.8). Nine patients had no previous HCC diagnosis or treatment, and the other 35 patients had treatment histories for HCC: percutaneous ethanol injection (PEI) in five, radiofrequency ablation (RFA) in 17, transarterial chemoembolization (TACE) in five and TACE followed by PEI in eight. Hypervascular lesions were located at treated sites in 43 lesions in 34 patients and at untreated sites in 12 lesions in 10 patients. As non-contrast-enhanced greyscale US examination had failed to detect any of the lesions, a percutaneous needle biopsy was not performed at that time. This study was approved by the ethics committee of our institute, and informed written consent was obtained from all patients.

Ultrasound examination

US examination was performed using SSA-770A and 790A (APLIO; Toshiba, Tokyo, Japan) with a 3.75 MHz convex or microconvex probe. After non-contrast greyscale US (tissue harmonic imaging, 2.5/5.0, 14–27 Hz) and colour Doppler imaging, contrast-enhanced US was carried out in the pulse subtraction harmonic imaging mode with an MI level from 0.24 to 0.3 to observe the suspected tumour location area as estimated from the contrast-enhanced CT images. Gain was adjusted at an optimal level, and the dynamic range was set at 65 dB for non-contrast US and 45-55 dB for contrast-enhanced US. Observation of non-contrast images and the late-phase (5–10 min after the injection of Sonazoid™) images was performed by both an intercostal scan and a subcostal scan for the right lobe, and both a sagittal scan and a transverse scan for the left lobe, under possible breath holding. Each scan was completed with gentle and reciprocatory movement of the probe, right side to left side and left side to right side, or caudal side to cranial side and cranial side to caudal side. As for the early phase (from onset of contrast enhancement to 1 min), a scan plane that allowed the most stable demonstration was carefully selected and contrast-enhanced findings were observed by tilting the probe under possible breath holding.

The contrast agent Sonazoid™ (perflubutane microbubbles with a median diameter of 2–3 μm) was used at a dose of 0.0075 ml/kg by a manual bolus injection following a flush with 3.0 ml of normal saline solution, once for the observation of each lesion (once in 37 patients, twice in four patients, three times in two

Liver International (2008)

patients and four times in one patient). The subsequent injection was given after the disappearance of the previous enhancement. The operators for US examinations were H. M. (18-year experience) in 20 patients, M. T. (6-year experience) in 14 patients, H. I. (6-year experience) in six patients and H. O. (8-year experience) in four patients. All US images recorded digitally were reviewed at a later date by H. O., and contrast-enhanced findings in the hepatic lesions were noted in comparison with those in surrounding liver parenchyma as positive, equal or negative enhancement. Hepatic lesions with either positive enhancement in the early-phase image or negative enhancement in the late-phase image were considered to be localized target lesions. Furthermore, the presence or absence of contrast enhancement in the intrahepatic portal vein was also noted at the late phase, based on the microbubble-disappearance time (20).

Contrast-enhanced computed tomography and computed tomography angiography

Contrast-enhanced CT with a dynamic study was performed in all patients using Lightspeed ultra16 (GE Yokogawa Medical Systems, Hino, Japan) with an injection of 100 ml of a contrast medium (Iopamiron 350; Nihon Schering, Osaka, Japan) at 3 ml/s from the antecubital vein by a mechanical power injector. Imaging was performed with a 30-s delay between contrast medium administration and start of imaging for the hepatic artery-dominant phase, an 80-s delay for the portal vein-dominant phase and a 180-s delay for the equilibrium phase. Contrast-enhanced CT was performed again in patients who received treatment for hepatic lesions to evaluate the therapeutic response. Findings of contrast-enhanced CT both before and after the treatment were evaluated blindly by S. O. to confirm the therapeutic effect and whether the lesion contrast-enhanced US demonstrated was the lesion detected on contrast-enhanced CT.

CT angiography was performed using Infinix Active Aquilion Type (Toshiba) with an injection of 15 ml of contrast medium (Iopamiron 300; Nihon Schering) at 3 ml/s via a catheter placed at the common hepatic artery by a mechanical power injector. Imaging was performed with a 2-s and an 8-s delay between contrast medium administration and start of imaging for the artery-dominant phase. This imaging was planned after a contrast-enhanced US examination and applied in 27 patients according to the standard protocol in our department: in patients with the initial treatment for HCC, patients with solitary or multiple lesions requiring TACE because of the lesions considered to be technically difficult for percutaneous needle advancement and patients with hepatic lesions not demonstrated by contrast-enhanced US. Findings of CT angiography were evaluated blindly by M. Y.

Ultrasound-guided puncture for hepatic lesions

Biopsy for hepatic lesions was performed by a 21-gauge needle (Sonopsy; Hakko, Tokyo, Japan), PEI was performed with a 22-gauge Chiba needle (Top, Tokyo, Japan) and RFA was performed with a 17-gauge cool-tip radio frequency electrode (Radionics, Burlington, MA, USA). All US-guided procedures were performed using a convex or micro-convex probe with a specially designed attachment. Percutaneous needle biopsy was applied in patients with the initial diagnosis or treatment for HCC, according to the standard protocol in our department. When hepatic lesions became recognized on the non-contrast sonogram in reference to the contrast-enhanced US findings, US-guided punctures were conducted under non-contrast US. However, when hepatic lesions were not clearly recognized on the non-contrast sonogram regardless of the reference of contrast-enhanced US findings, these US-guided procedures were conducted under contrast-enhanced US with an additional injection of Sonazoid™.

Statistical analysis

All data were expressed as mean ± standard deviation or percentage. Statistical significance was determined using Fisher's exact test, and significance was considered at $P < 0.05$. Statistical analysis was performed using the SPSS package (version 13.0J; SPSS Inc., Chicago, IL, USA).

Results

Detection of focal hepatic lesions by contrast-enhanced ultrasound

Fifty-two lesions showed a positive enhancement in the early phase and 44 lesions showed a negative enhancement in the late phase (Table 1), with phasic detectability being significantly higher in the early phase (52/55) than that in the late phase (44/55, $P = 0.0221$). Consequently, 53 lesions were demonstrated by contrast-enhanced US with Sonazoid™, yielding a detection rate of 96.4% (Figs 1 and 2). Twenty-one of the 55 lesions (38.2%) were < 10 mm, with the detection rate between lesions < 10 mm and ≥ 10 mm not being significantly different (Fig. 3). In addition, 13 of the 55 lesions (23.6%) lesions were located deeper than 8 cm from the skin surface (Fig. 3). Contrast enhancement in the intrahepatic portal vein at the late phase was still visible in 33 (60%) patients with 37 lesions and in 11 (29.7%) of the 37

Table 1. Contrast-enhanced ultrasound findings of hepatic lesions in each phase

Enhanced findings	Early phase	Late phase
Positive	52	0
Equal	3	11
Negative	0	44

Fifty-two lesions showed positive enhancement in the early phase and 44 lesions showed negative enhancement in the late phase, with phasic detectability being significantly higher in the early phase (52/55) than in the late phase (44/55, $P=0.0221$). Consequently, 53 lesions were demonstrated by contrast-enhanced ultrasound with Sonazoid™, a detection rate of 96.4%.

lesions showing an equal enhancement to the surrounding liver parenchyma in this phase. Percutaneous needle biopsy was performed for 10 of the successfully demonstrated 53 lesions under the non-contrast sonogram. Their diagnosis was seven moderately differentiated HCC (7, 10, 13, 15, 18, 20 and 24 mm), two well-differentiated HCC (10, 12 mm) and one benign nodule (13 mm) found in alcoholic liver disease.

Clinical course after contrast-enhanced ultrasound

Percutaneous US-guided treatments were successfully performed in 42 lesions (PEI in 20 and RFA in 22) in 32 patients, and all hypervascular hepatic lesions changed to hypovascular appearances

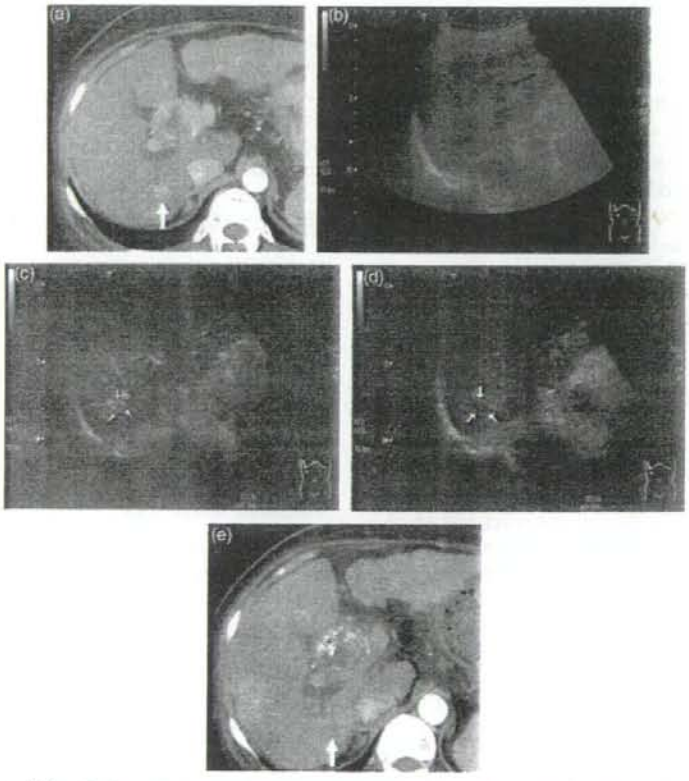

Fig. 1. Fifty-seven-year-old female, hepatitis B virus-related liver cirrhosis. (a) Contrast-enhanced computed tomography (CT) image. A hypervascular lesion (arrow) considered to be hepatocellular carcinoma was demonstrated on CT image. (b) Non-contrast sonogram. Hepatic lesion corresponding to CT findings was not recognized on the sonogram before enhancement. (c) Contrast-enhanced sonogram in the early phase. A hypervascular lesion was demonstrated on the sonogram after enhancement (arrows). (d) Contrast-enhanced sonogram in the late phase. The lesion showed negative enhancement in this phase (arrows). (e) Contrast-enhanced CT image after a percutaneous ethanol injection. Hepatic lesion showed a hypovascular appearance after the treatment (arrow).